fire

MDPI

Review

Fire and Explosion Safety of Battery-Electric Mining Vehicles: A Multi-Scale Review from Cell to Ventilation Network

Shimin Liu [1], Dejian Wu [2,*], Liwei Zhang [1,*] and Yufang Song [1]

[1] School of Fire Protection Engineering, China People's Police University, Langfang 065000, China
[2] School of Emergency Management and Safety Engineering, China University of Mining and Technology-Beijing, Beijing 100083, China
* Correspondence: dejian.wu@cumtb.edu.cn (D.W.); zhangliwei02@cppu.edu.cn (L.Z.)

Abstract

Battery failure in underground mining vehicles can expose connected workings to heat and hazardous gases. This review synthesises research published primarily between 2010 and 2026 on battery thermal runaway, enclosure response, underground hazard transport and emergency response. It finds that propagation and gas release can continue without sustained external flames, while enclosure pressure and downstream exposure depend on release history, discharge conditions and ventilation. Methane and entrained coal dust may introduce additional explosion pathways under suitable mixing and ignition conditions. Intervention also depends on the failure stage, because electrical isolation cannot stop self-sustaining cell reactions. A key gap remains between pack and enclosure measurements and the changing conditions encountered by mine personnel. To address this gap, this review proposes a cross-scale assessment framework linking battery monitoring and thermal management with enclosure performance, ventilation response and personnel protection. The framework identifies the source inputs and validation checks required at each interface and relates hazard development to intervention timing, personnel movement and usable self-rescuer endurance to assess escape-route viability.

Keywords: battery-electric mining vehicles; lithium-ion batteries; thermal runaway; battery thermal management; fire and explosion hazards; ventilation networks

1. Introduction

The electrification of underground mining equipment is rapidly expanding from small auxiliary units to heavy-duty machinery, including load–haul–dump (LHD) vehicles, mine haul trucks, drilling rigs, loaders, and personnel carriers. Compared with conventional diesel-powered equipment, battery-electric vehicles (BEVs) significantly reduce emissions of diesel particulate matter (DPM), CO, and NO_x, as well as waste heat from exhaust gases. Consequently, their adoption can lower ventilation and refrigeration demand in deep mines while simultaneously eliminating the operating constraints imposed by trailing cables [1–3]. A recent simulation-based study at Turquoise Ridge Mine further showed that BEV operation can support the effective implementation of ventilation-on-demand in an underground metal mine [1]. However, electrification does not remove the mechanical, electrical, and access hazards of underground mining. Battery failure can introduce additional hazards from thermal runaway, pressure development, and

Academic Editor: Qingsong Wang

Received: 17 September 2026
Revised: 20 October 2026
Accepted: 31 October 2026
Published: 1 November 2026

Copyright: © 2026 by the author. Licensee MDPI, Basel, Switzerland. This article is an open access article distributed under the terms and conditions of the Creative Commons Attribution (CC BY) license.

flammable and toxic gas release. Depending on the discharge and ignition conditions, these releases may produce jet flames or ignite after a period of accumulation [4–6].

The confined geometry and ventilation conditions of underground mines can substantially amplify the consequences of a battery fire. Mining vehicles routinely operate in haulage roadways, declines, production headings, charging chambers, and maintenance areas with restricted cross-sections. Limited access points, complex branching roadways, and continuously operating ventilation systems allow hot smoke and toxic products to spread from the vehicle to downwind working areas. A burning or immobilised vehicle may also obstruct a narrow roadway, blocking evacuation and rescue routes [7,8]. Fire consequences therefore depend not only on battery capacity and fire intensity, but also on the fire location, roadway network, ventilation direction, distribution of personnel, and availability of escape routes. For non-coal underground mines, established guidance identifies fire location, ventilation conditions, and access to safe locations as key determinants of fire risk [9]. The additional escalation pathways depend on the fuels and conditions at the site. Methane and airborne coal dust may introduce further explosion pathways in gassy coal mines. Battery vent-gas accumulation, ignition of vehicle materials, toxic exposure, and roadway obstruction also remain relevant in metal and non-metal mines. Where flammable gases or combustible mineral dusts are present, these need to be considered alongside the battery release. Hazard scenarios should therefore be defined from the actual fuels, ventilation, and roadway conditions.

The duty cycles and environmental exposures of mining vehicles create battery-failure conditions that differ from those encountered in conventional road vehicles. Heavy-load climbing, frequent acceleration and braking, regenerative braking, and fast charging produce large current transients and repeated thermal loading. Continuous vibration, mechanical shock, and vehicle collisions may loosen electrical connections, deform enclosures, damage cooling circuits, and initiate latent internal short circuits [10,11]. High temperature and humidity, dust, water ingress, and corrosive contaminants can further accelerate battery ageing, insulation degradation, and seal deterioration [2,12,13]. Laboratory tests of temperature and vibration effects have measured changes in discharge capacity and internal resistance under defined loading conditions [14]. A review of degradation mechanisms further shows that cell ageing depends on operating history and interactions between processes [15]. Together, this evidence supports consideration of interacting service loads, but changes in capacity or resistance alone do not establish when an internal short circuit or thermal runaway will occur.

Lithium-ion battery thermal runaway begins when internal heat generation exceeds heat dissipation. Mechanical deformation, short circuits, overcharge, overheating, manufacturing defects, lithium plating, and ageing may all disturb this balance [16–19]. Once initiated, thermal runaway releases heat, flammable and toxic gases, pressure pulses, hot jets, and solid particles [20]. Battery chemistry, state of charge (SOC), and ageing condition influence the initial source term, while cell arrangement, electrical configuration, cooling, free volume, and venting govern its development within the pack. Sequential or near-simultaneous cell failures can produce intermittent and highly directional releases. Pack-level heat, gas, and pressure behaviour therefore cannot be estimated by simply multiplying single-cell measurements by the number of cells [21].

A further challenge arises from the use of flameproof enclosures in underground coal mines. These enclosures are intended to withstand an internal explosion and prevent flame transmission to an external methane–air atmosphere. Battery failure can impose heat and gas loads that continue beyond an individual ignition event. Heating of neighbouring cells and gas discharge also need to be considered when no sustained external flame is present. Restricted discharge can increase internal thermal and pressure loads, while the discharged gases create a separate hazard outside the enclosure. Tests of cells

within sealed enclosures have shown the dependence of thermal-runaway pressure on available free volume [22,23], and a test in a modified explosion-proof enclosure recorded deformation and jet flames emerging from its cover joint [24]. Pack assessment therefore needs to address both the loads retained inside the enclosure and the gas, heat, and potential ignition sources discharged into the roadway.

In a gassy coal mine, battery gases released from the enclosure may mix with methane, coal dust, and electrolyte aerosols. Typical vent products include H_2, CO, CH_4, C_2H_4, CO_2, HF, and other fluorinated species, although their composition varies with battery chemistry, state of charge, and failure conditions [25–28]. Local accumulation can result in delayed ignition. Methane changes the composition and combustion behaviour of the gas mixture, while an initial pressure wave may lift deposited coal dust and add further fuel. These interactions can produce a hybrid hazard that cannot be evaluated from the concentration of methane, coal dust, or battery vent gases alone. This methane–coal-dust coupling is not representative of every underground mine, although vent-gas ignition, toxic exposure, and confined smoke transport remain relevant in both coal and metal/nonmetal operations.

Ventilation influences both the development and the spatial consequences of the incident. Airflow affects the dilution and transport of an unignited gas release. Where combustion occurs, it also supplies oxygen and carries hot smoke into downwind workings. Smoke backlayering, local recirculation, and airflow redistribution may develop as a result of plume buoyancy, roadway inclination, vehicle blockage, and fire-induced pressure [7,8]. Route assessment therefore needs to account for the ventilation conditions as they develop during the incident. Hazard arrival times and local conditions must then be compared with the times at which personnel are expected to pass through each route segment. An incident in an intake decline, charging chamber, or critical intersection may affect several branches and restrict escape where airways or access routes are shared.

Previous reviews have examined lithium-ion battery technology, thermal runaway and enclosure protection for mining applications [2]. Hooli and Halim combined information on underground BEV deployment and reported fire incidents with surveys of mine management and personnel [3]. Kuslap et al. reviewed the benefits, operating challenges and safety considerations of underground BEVs [6], while Said et al. examined large-format battery thermal runaway, detection and mitigation in underground operations [13]. Table 1 compares the scope of these publications and identifies the assessment questions pursued here. Building on this work, the present review examines how evidence on battery failure and enclosure discharge can inform assessments of roadway transport, ventilation-network contamination and personnel response. It follows both burning and unignited releases, with attention to the conditions required when applying findings from one scale at another. Figure 1 outlines these pathways and the checks used to assess evidence applicability.

Table 1. Scope of selected reviews and industry research in relation to the present assessment.

Publication	Main Focus	Main Scales or Assessment Levels	Mine Context	Question Pursued in the Present Review
Meng et al. [2]	Battery technology, thermal runaway and enclosure protection	Cell, pack, enclosure and equipment	Coal-mine emphasis, with non-coal applications also discussed	How pack and enclosure findings can define the release entering a roadway
Hooli and Halim [3]	Deployment, reported fire incidents and stakeholder experience	Vehicle and mine operation	Underground mine deployments and trials	What physical evidence is needed to assess the reported fire-safety concerns

Kuslap et al. [6]	Battery selection, deployment benefits and safety challenges	Cell chemistry, vehicle and mine operation	Underground mining, including metal-mine examples	How incident releases affect local conditions and exposure through connected workings
Said et al. [13]	Thermal runaway, detection, mitigation and emergency handling	Cell, module, pack and emergency response	Underground mining, including coal-mine explosion hazards	How warning and mitigation results relate to continuing release and available response time
Present review	Evidence linking battery failure, discharge, transport and personnel protection	Cell, module, pack, vehicle, roadway and ventilation network	Coal and metal/non-metal mines, with site-dependent escalation pathways	Under what conditions evidence supports the next assessment scale and the required protective action

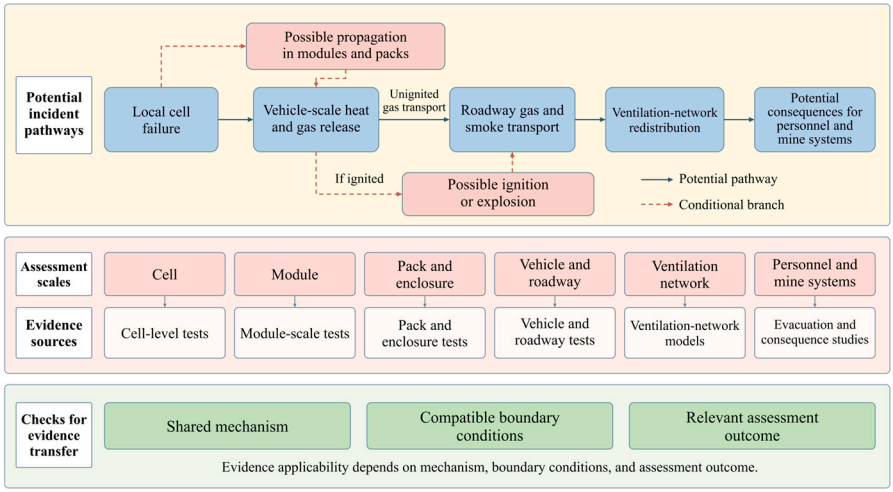


Figure 1. Assessment scales, potential incident pathways, and evidence sources for battery-electric mining vehicle incidents. The schematic includes transport of unignited releases and conditional propagation and ignition pathways. Evidence applicability is assessed through the mechanism, boundary conditions, and outcome of interest.

This review addresses three questions. First, which mining-related failure conditions and release pathways govern escalation from cells to packs, enclosures and vehicles? Second, under what conditions can experimental measurements and model results support assessment of roadway transport and ventilation-network contamination? Third, how can the resulting hazard histories inform intervention timing, escape-route viability and personnel protection? To answer these questions, experimental observations, model predictions and proposed protective measures are examined separately, with attention to their mechanisms, boundary conditions and assessment outcomes. Methane and coal-dust involvement is considered where the relevant fuels and enabling conditions are present.

2. Literature Search Strategy and Scope

This study is a structured narrative review of fire and explosion safety in battery-electric underground mining vehicles. It combines a documented database search with purposive selection of evidence relevant to the progression from cell failure to mine-wide consequences. The synthesis examines failure mechanisms, boundary conditions and the applicability of protective measures. The heterogeneity of the experimental configurations, numerical models and regulatory sources precludes a pooled effect estimate or a quantitative ranking of accident likelihood.

2.1. Search Strategy and Coverage

The databases searched were the Web of Science Core Collection, Scopus and Compendex through Engineering Village, with database year limits set to 2010–2026. The final database searches were completed on 12 October 2026. Web of Science records dated 2026 in the Early Access field were retained in the exported search library even when their final publication year was listed as 2027. Searches used Topic fields in Web of Science, TITLE-ABS-KEY in Scopus and Subject/Title/Abstract fields in Compendex.

Six complementary themes covered mining vehicles and batteries; thermal runaway, fire and vent-gas release; confinement and explosion-proof enclosures; methane–coal-dust and other combustible hybrid mixtures; roadway smoke, ventilation and evacuation; and detection, thermal management and suppression. These themes were searched separately to capture both battery-failure studies and mine-environment studies without requiring every record to contain both battery and mining terminology. The mining-vehicle search combined battery and electric-vehicle terms with mining, underground-mine and mining-equipment terms. The hybrid-mixture search combined methane, coal dust, hybrid-mixture and gas–dust terms with explosion, ignition and flame-propagation terms. The roadway search combined mine or tunnel terms with fire, smoke or carbon monoxide, and ventilation, backlayering, stratification, evacuation or tenability terms.

A representative Web of Science query for confined battery hazards was TS=("lithium-ion batter*" OR "lithium ion batter*" OR "Li-ion batter*" OR "lithium-ion cell*" OR "lithium ion cell*" OR "Li-ion cell*") AND TS=(flameproof OR "explosion-proof" OR "explosion proof" OR enclosure* OR confin* OR "pressure relief" OR "flame arrest*") AND TS=("thermal runaway" OR fire* OR explos* OR pressure OR "gas release") AND PY=(2010–2026). Corresponding term groups were used with the Scopus and Compendex search fields; Scopus year limits were PUBYEAR > 2009 AND PUBYEAR < 2027.

Earlier foundational sources were identified through backward and forward citation tracking. Targeted publisher and institutional searches supported source verification and supplementary discovery. Standards and guidance were obtained from their issuing organisations and considered separately from research findings.

2.2. Source Selection and Evidence Appraisal

The archived exports contained 34,698 Web of Science entries, 46,977 Scopus entries and 35,475 Compendex entries, totalling 117,150 exported entries. Matching database-specific identifiers across thematic searches and export batches reduced these to 29,739, 31,361 and 30,200 records, respectively. Cross-database deduplication then used valid normalised DOIs, followed by exact normalised title–year matching with checks for compatible document types and, where available, volume, issue, first-page and article-number information. Title normalisation accounted for letter case, Unicode characters and punctuation. Short article titles additionally required matching author and source information, while generic proceedings-series titles required edition information rather than title–year matching alone. Records with conflicting DOIs or unresolved bibliographic relationships were retained separately. Within-database matching removed 25,850 duplicate entries, leaving 91,300 records across the three databases. Cross-database deduplication removed a further 46,478 entries. In total, 72,328 duplicate entries were removed from the 117,150 exported entries, leaving 44,822 records in the working search library. The 44,822 records formed a bibliographic search pool rather than a set of included studies. The final synthesis drew on 126 cited source documents identified through database searching, citation tracking and targeted source verification. These comprised 115 research publications, reviews and handbook chapters, nine standards, regulations and guidance documents, and two conference presentations reporting operational incidents.

Sources were selected purposively within the six themes. Titles, abstracts and keywords guided the identification of studies addressing battery-failure initiation, propagation, heat and gas release, pressure development, ignition, smoke transport, ventilation response, evacuation or protective barriers. Primary reports were consulted for the experimental conditions and outcomes supporting quantitative statements. Studies concerned only with electrode performance, resource extraction, vehicle economics or driving range were excluded unless they established a relevant safety mechanism or operating constraint. General gas–solid studies were retained only when they informed combustible hybrid-mixture behaviour. Reviews provided context and routes to primary studies. Publications describing the same experimental series or model dataset were treated as related reports rather than independent corroboration. Abstract-only information supported discovery and qualitative scope assessment, but was not used to establish numerical design limits.

Evidence appraisal considered source traceability, reporting of boundary conditions, clarity of the outcome being assessed, and the credibility of measurements or model validation. Experimental interpretation considered battery chemistry, format, capacity, state of charge (SOC), ageing, initiation method, electrical configuration, cell spacing, thermal contact, confinement, free volume, venting, atmosphere, airflow, instrumentation and replication where reported. Absolute and gauge pressures were distinguished. Vent opening, gas release, thermal-runaway onset, ignition and detector response were treated as separate endpoints, with the reported definitions and timing used to interpret each result. A gas-release-to-thermal-runaway interval was therefore not assumed to represent an available alarm lead time.

For numerical studies, appraisal considered source-term assumptions, boundary conditions, spatial and temporal resolution, sensitivity analysis, uncertainty treatment and comparison with relevant measurements where available. Calibration against an experimental trace was distinguished from independent validation. A model's applicability was assessed against the physical processes and output quantities it resolved; agreement at one scale or for one endpoint was not taken as validation of the complete accident sequence.

Evidence appraisal was qualitative and specific to the claim being evaluated, without numerical quality scores or statistical weighting. Research findings with explicit boundary conditions, clearly defined outcomes and relevant measurement or validation support were given greater interpretative weight. Experimental observations, numerical predictions and proposed mechanisms were distinguished when drawing conclusions. The same principle guided the use of other source types: standards established requirements and test boundaries, while incident reports informed accident scenarios without providing a basis for estimating failure frequencies or intervention effectiveness.

2.3. Evidence Applicability Across Scales

Application context and physical scale were assessed separately. Direct mining evidence comprised mining-equipment tests, mining-specific enclosure investigations, mine-roadway studies and analyses of actual mine networks. A mining-specific cell or enclosure experiment remained evidence at its tested scale and did not establish complete-vehicle safety. Generic cells and modules, road vehicles, stationary storage, road tunnels and car parks provided indirect evidence. Mining relevance alone did not determine evidential quality: measurement credibility, boundary conditions and the quantity being inferred remained necessary considerations. Indirect evidence could support a shared physical mechanism, while its use for mining design values required additional justification.

Cross-scale interpretation followed three checks: whether the source and target shared the governing mechanism; whether their material, geometric and operating

conditions matched or could be related through a validated model; and whether the required output quantity had actually been measured or resolved. These checks were applied to individual claims rather than assigning an entire publication a single level of applicability.

Evidence was used in four ways. Quantitative findings were retained within demonstrated conditions or a validated transfer relationship. Findings sharing a mechanism but differing in boundary conditions provided qualitative mechanistic support. Values introduced into an unmatched application were identified as explicit scenario assumptions, with their conditions and limitations stated. Transitions lacking the required variables, processes or validation were identified as evidence gaps. Agreement among studies strengthened a conclusion when their conditions and outcomes were comparable; discrepancies were examined against those conditions rather than averaged across incompatible tests.

The synthesis included both flaming and non-flaming thermal-runaway pathways. For flaming events, evidence was examined in relation to heat release, combustion products and smoke transport. For non-flaming events, the assessment addressed unignited gas and electrolyte-vapour release, accumulation and potential delayed ignition. Cross-scale applicability was evaluated against the release history, ignition state, confinement and ventilation conditions relevant to the target scenario. Table 2 summarises the information required at successive transitions and the principal restrictions on transferring evidence.

Table 2. Conditions governing the use of evidence across scales in this review.

Transition	Information Required	Use and Principal Restriction
Cell to module or pack	Chemistry, capacity, SOC, ageing, failure trigger, electrical connections, spacing, thermal contact, cooling and propagation sequence	Cell tests inform initiation and local mechanisms. Pack release histories require propagation evidence; cell outputs cannot simply be multiplied by cell count.
Pack to enclosure or vehicle	Gas-generation history, free volume, vent area and resistance, seal behaviour, pressure response and secondary vehicle fuels	Confinement results apply to the tested assembly. Sealed-cell pressures do not establish pressure limits for an untested pack or vehicle.
Vehicle to roadway	Time-dependent heat and species release, ignition state, discharge direction and momentum, blockage, geometry and airflow	Transport calculations require compatible source terms. A steady isotropic fire source does not represent a directional vent jet or an unignited release.
Vent gas to delayed ignition	Gas and vapour composition, release rate, dilution, accumulation, ignition timing and methane or coal dust where present	Fire-smoke results alone do not establish cloud flammability or explosion loads. Ignition and pressure development require suitable evidence or validation.
Roadway to mine network	Heat and contaminant fluxes, fire-induced pressure, branch resistance, fans, doors and transient airflow	Network models address redistribution within their assumptions. Local stratification and rapid explosion-pressure waves require separate resolution.
Network to evacuation	Route-specific exposure, visibility, temperature, detection and mobilisation delays, travel time, refuge access and self-rescuer endurance	Exposure and escape calculations require a common time basis. Smoke arrival alone does not establish toxic dose, tenability or successful escape.

3. Mining Vehicle Duty Cycles and Operating-Environment Stressors

Battery-electric vehicles in underground mines typically operate under high loads, at low speeds, with frequent starts and stops, and over inclined haulage routes. Starting under heavy load, sustained uphill travel, and wheel slip can produce high or transient discharge currents. Joule heating and electrochemical polarisation heat may therefore accumulate over repeated haulage cycles when heat rejection is insufficient [15,29]. During long downhill runs, regenerative braking rapidly switches the battery from discharge to charge. At a high state of charge or low temperature, the battery becomes less able to accept regenerative power, increasing charge polarisation and the risk of lithium plating [30,31]. Braking energy that exceeds the battery's charge-acceptance limit must be

dissipated by the mechanical braking system. The resulting high temperatures can impose additional thermal exposure on nearby cables, hydraulic lines, and the battery compartment.

Battery-electric mining vehicles commonly use fast charging, opportunity charging, or battery swapping to minimise downtime. Charging immediately after continuous operation can expose an already warm battery to additional electrical and thermal loading. Elevated temperature accelerates interfacial side reactions and thermal ageing. Lithium plating instead becomes more likely when the charging current exceeds the local capacity for lithium intercalation, particularly at low temperature, high state of charge, or under transport limitations. Temperature non-uniformity can further concentrate these effects within the pack. Qu et al. tested commercial 18650 lithium nickel manganese cobalt oxide (NMC) cells at charging rates of 1 C, 3 C and 5 C and operating temperatures of 25 and 40 °C. Within these conditions, increasing temperature partly alleviated capacity fade at higher charging rates but accelerated it at lower rates, with the dominant degradation mechanism shifting from lithium plating towards growth of the solid electrolyte interphase (SEI) [32]. Charging limits therefore need to account for both heat-driven degradation and the local electrochemical conditions associated with plating [12,30–32]. Opportunity charging introduces repeated partial charge–discharge cycles within a single shift, accompanied by frequent changes in state of charge, temperature, and current. Battery swapping also increases connector wear and the likelihood of terminal contamination or poor electrical contact. As contact resistance rises, terminals, busbars, and high-voltage connectors may develop localised heating even when the average cell temperature remains within its allowable range. Inadequate grounding, insulation ageing, or poor coordination between the charger and battery management system (BMS) may also cause overcharge, abnormal current, or electrical arcing [4].

Potholes, loose rock, roadway joints, and standing water expose heavy mining vehicles to prolonged random vibration and intermittent shock. Mechanical energy transmitted through the vehicle frame and battery mounting structure can loosen fasteners, fatigue welds, crack busbars, abrade wiring harnesses, and displace cooling-line connections. These changes can alter both the electrical connections and heat-transfer conditions within the pack [10,11]. Slight deformation of a cell casing, local compression of the separator, or electrode misalignment may initially produce no clear voltage or temperature anomaly. Under subsequent cycling and vibration, however, such damage can gradually develop into an internal micro-short circuit [11,33]. A vehicle collision may simultaneously reduce cell spacing, damage the cooling circuit, displace thermal barriers, and obstruct venting paths. Internal short circuit, impaired heat dissipation, and restricted venting may then develop as a continuous failure sequence. Zhang et al. measured discharge capacity and internal resistance in 18650 cells of 2.9 Ah with lithium nickel cobalt aluminium oxide (NCA) cathodes under controlled temperature and vibration conditions, with temperature having the largest influence in their orthogonal comparison [14]. These endpoints support assessment of electrical performance under the tested conditions; mechanically initiated faults and thermal-runaway thresholds require structural and thermal failure tests under representative mining loads.

Temperature, humidity, and dust conditions vary considerably across underground mine workings and act alongside the duty-cycle and mechanical stressors compared in Table 3. Sustained high temperatures accelerate electrolyte decomposition, solid electrolyte interphase growth, and loss of active lithium, resulting in capacity fade and increased internal resistance. By contrast, high-rate charging at low temperatures increases the risk of lithium plating at the anode [15,30,31]. Repeated temperature changes also produce differential thermal expansion among cells, busbars, sealing materials, and the enclosure. Moisture entering the battery compartment through aged seals, damaged connectors, or

pressure-equalisation devices can combine with conductive mine dust, reducing insulation resistance and accelerating corrosion of terminals and connections. Deposits of coal dust, metallic mineral dust, or rock dust on heat exchangers, air passages, and connectors can impair heat transfer and increase temperature non-uniformity within the pack. Conductive dust entering high-voltage regions may also create creepage paths or local short circuits [13].

Table 3. Mining duty-cycle and environmental stressors, potential faults, candidate indicators and proposed validation conditions.

Mining Stressor	Battery or Pack Response	Potential Latent Fault	Candidate Indicator	Proposed Validation for Mining Use
Heavy-load starting and uphill haulage	High current and repeated heat accumulation [15]	Accelerated ageing; local overheating	Temperature-rise rate; voltage deviation; internal-resistance growth	Repeated high-load duty cycles [3]
Regenerative braking	Rapid transition from discharge to charge [30,31]	Lithium plating under limited charge acceptance	Charge-current peak; voltage imbalance; temperature change	High-SOC and low-temperature braking [30,31]
Fast and opportunity charging	High electrochemical and thermal load before complete cooldown [12,30–32]	Lithium plating; gas generation; interface degradation	Temperature difference; impedance change; capacity loss	Repeated charging at different initial temperatures and SOCs [12,30–32]
Connector wear and contamination	Increased contact resistance [4]	Local terminal or busbar heating; electrical arcing	Contact-resistance growth; intermittent voltage fluctuation	Repeated connection cycles under dust and moisture exposure [4]
Continuous vibration	Fatigue of fasteners, busbars, welds and cooling connections [10,11,14]	Loose electrical contact; coolant leakage; impaired heat transfer	Resistance fluctuation; pressure loss; local temperature difference	Long-duration, multi-axis vibration [10,11,14]
Collision, rock impact or floor contact	Cell, module or enclosure deformation [11]	Separator damage; internal micro-short circuit; displaced barriers	Strain; deformation; insulation change; pressure variation	Representative impact locations and mechanical boundary conditions [11,19,33]
High or low temperature	Accelerated side reactions or reduced charge acceptance [15,30,31]	Internal-resistance growth; lithium plating; capacity loss	Temperature history; impedance and capacity change	Thermal cycling combined with charging and discharge loads [6,15,34]
Dust, moisture and water ingress	Corrosion, insulation deterioration and blocked heat-transfer paths [13]	Leakage current; creepage path; cooling degradation	Insulation resistance; sensor drift; coolant or moisture detection	Combined dust–humidity and water-ingress exposure [13]

Operational loads, structural damage, and environmental exposure reinforce one another throughout the service life of the vehicle. Capacity loss requires deeper discharge or more frequent charging to complete the same haulage task, while increased internal resistance generates additional heat under high-current conditions. Vibration can enlarge gaps in seals and weaken electrical connections; subsequent ingress of moisture and dust further accelerates corrosion and insulation degradation [11,14,15]. As summarised in Figure 2, these interactions follow three main pathways: electrochemical ageing and internal-resistance growth; localised contact heating and micro-short circuits; and degradation of seals, corrosion resistance, and electrical insulation. Whether these faults initiate thermal runaway depends on the damage mechanism and the resulting local thermal balance [33,34]. In 24 Ah NMC/graphite pouch cells subjected to four ageing pathways, Ren et al. combined post-mortem analysis with adiabatic thermal testing and identified lithium plating as a key cause of deteriorating thermal-runaway behaviour [34]. At the mine-system scale, Eroglu et al. combined system dynamics modelling with HaulSim and VentSim to assess interactions among operational practices, battery use and environmental

stressors [35]. Their model outputs can inform operating scenarios for battery assessment, while fault-initiation thresholds require physical evidence at the relevant cell or pack scale.

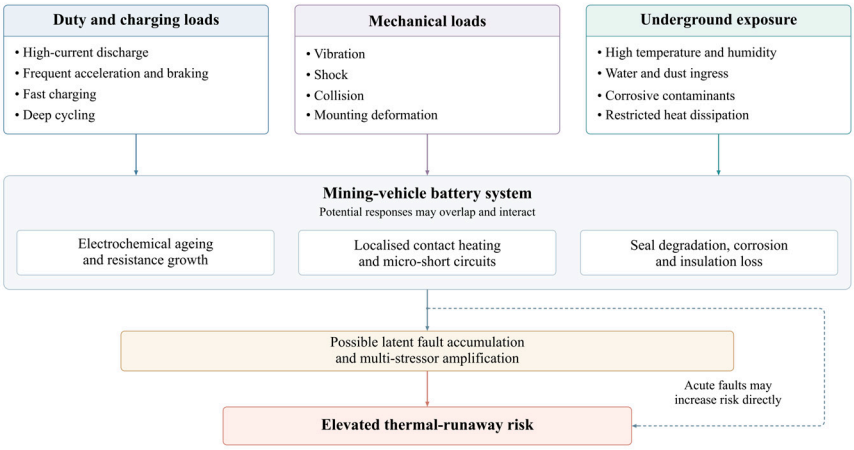


Figure 2. Battery-system degradation and failure mechanisms induced by the coupling of mining vehicle duty loads and underground environmental stressors.

4. Thermal-Runaway Source Terms in Battery Packs and Challenges for Flameproof Enclosures

4.1. Thermal, Gaseous, and Particulate Source Terms

Thermal runaway develops when internal heat generation from exothermic reactions exceeds heat removal. Its initiation and reaction sequence depend on cell chemistry, SOC, ageing and the abuse condition. An internal short circuit is one possible trigger, while electrode–electrolyte reactions, separator changes and, in some nickel-based cells, cathode oxygen release can contribute at different stages [17–19,36]. Cell thermal runaway, ignition of vent gases and sustained external burning are therefore treated as separate events.

For burning releases, calorimetry provides the external heat-release history; its peak, duration and integral describe different aspects of the thermal exposure [37,38]. Shen et al. monitored electrical, thermal and mechanical responses during externally heated failure of a 228 Ah mining battery, then used gas-composition data in numerical analyses of combustion and explosion characteristics at different release stages [39]. The measured responses characterise battery failure, whereas the calculated mixture behaviour applies to the compositions and reaction conditions represented in the simulations. Battery chemistry, SOC, construction and initiation conditions must consequently accompany heat-release comparisons [39,40]. Venting, thermal-runaway onset and external ignition also require separate time references when interpreting the signal sequence illustrated in Figure 3.

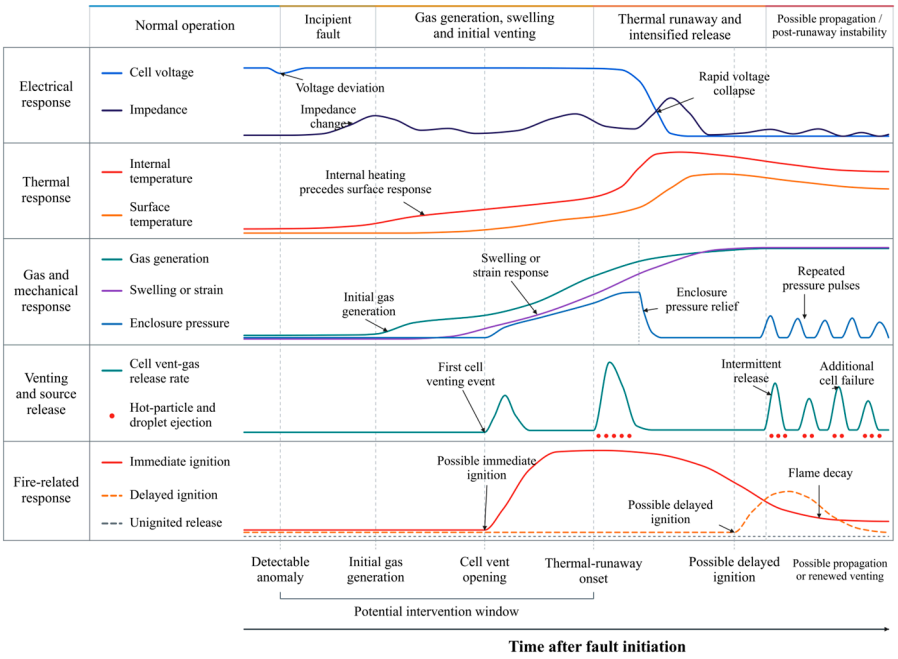


Figure 3. Conceptual evolution of multi-parameter warning signals and hazard source terms from incipient battery fault to thermal runaway, propagation, or reignition. The relative timing and magnitude of the signals are illustrative and depend on battery chemistry, state of charge, cell format, failure mode, confinement, and measurement location. Based on Refs. [17,28,41].

Vent gases released during thermal runaway are produced mainly by electrolyte evaporation and the decomposition of electrodes, electrolyte components, and binders. Typical constituents include H_2, CO, CO_2, CH_4, C_2H_4, and other low-molecular-weight hydrocarbons [28,41]. Their composition and yield vary with battery chemistry, state of charge, initiation temperature, and sampling stage. A high state of charge generally leads to a more severe reaction and a larger release of flammable gases. Differences among cathode chemistries, however, should not be interpreted as evidence that any particular chemistry is inherently safe [40,42,43]. Under open conditions, a lithium iron phosphate (LFP) cell may undergo thermal runaway without producing a sustained visible flame. Its unburned vent gases can nevertheless accumulate within an enclosed or partially enclosed space and reach a flammable concentration. Yuan et al. combined accelerating rate calorimetry (ARC) with gas chromatography to characterise cell thermal response and vent-gas composition [44]; these endpoints need to be distinguished from external heat-release rate (HRR) and jet-flame length. Immediate ignition of vent gases primarily produces jet flames and thermal radiation, whereas delayed ignition may create a larger flammable cloud and a more severe pressure event [26,45].

Decomposition of fluorinated electrolytes and lithium salts also produces toxic and corrosive compounds, including HF and POF_3. The quantities released depend on battery chemistry, state of charge, combustion conditions, and the presence of moisture [25,28]. Heat release, flammable and toxic gases, pressure, jet flames, and ejected particles collectively define the source terms of a mining-battery incident. The experimental results compared in Table 4 illustrate how battery characteristics, initiation methods, and confinement influence the measured source terms and their applicability to mining conditions. Larsson et al. measured HF emissions of approximately 20–200 mg/Wh from fires involving different commercial lithium-ion batteries. They also found no consistent relationship between HF release and visible flame intensity [25]. Thermal-runaway jets may entrain metal fragments, graphite particles, and electrolyte droplets, creating mobile heat sources or potential ignition sources both inside and outside the battery pack. Rapid gas

generation combined with inadequate venting can rupture the cell casing and eject particles at high velocity [46]. These observations show that the hazard zone can extend well beyond the physical dimensions of the battery system and that no single precursor can capture every stage of escalation; electrical, thermal, gas, pressure, and impedance signals should therefore be interpreted together [21,47–50].

Transfer to a roadway model requires source terms at the discharge boundary. A burning release requires an external combustion heat-release history and appropriate combustion-product rates. An unignited release requires the gas and vapour mass-flow history, composition, temperature, direction and momentum. Where gas-phase mass flow and constituent mass fractions are available, the outlet species source is expressed as

$$\dot{m}_{i,out}(t) = Y_{i,out}(t)\,\dot{m}_{gas,out}(t) \quad (1)$$

where $\dot{m}_{i,out}(t)$ is the outlet mass-flow rate of constituent (i), $Y_{i,out}(t)$ is its gas-phase mass fraction, and $\dot{m}_{gas,out}(t)$ is the total gas-phase mass-flow rate. The composition must include diluting species and use a consistent mass basis; aerosol discharge requires separate treatment. A reported total gas volume constrains the released inventory but does not determine its transient release rate [28,41]. Internal reaction heat, external-heater input and combustion heat must also be distinguished when constructing the thermal source.

Table 4. Comparison of representative experimental studies on thermal-runaway release, confinement, and scale-dependent hazards.

Study	Battery and SOC	Initiation	Scale and Boundary Conditions	Principal Result	Implication for Transfer
Dubaniewicz et al. [23]	NMC811, 3.2 Ah; 100% SOC	ARC heating	Single cell; sealed canister; 92.5 mL free space in the reported case	Approximately 232 bar absolute pressure	Interpretation requires the tested free volume, cell construction and confinement
Dubaniewicz et al. [23]	NMC pouch, 100 Ah; 100% SOC	ARC heating	Form-fitting enclosure with pressure relief and observed leakage	Approximately 29.4 bar absolute pressure before abrupt relief	Pressure reflects relief behaviour, leakage and thermal contact
Amano et al. [45]	NMC pouch, 2.5, 10 and 32 Ah; SOC varied; overcharge tests exceeded 100% SOC	Local heating, heating plate or overcharge	Single cells and two-cell stacks; 10/100 L vessels and a 45 L chamber	Calculated mixture limits: approximately 7 vol% LEL and 31 vol% UEL	Composition-based calculations require scrutiny of sampled components and test conditions
Tschirschwitz et al. [21]	NMC cells, stacks and second-life modules; 2.65/6.85 kWh modules; near 100% SOC	Heating or overcharge	Cell-to-module tests with differing opening conditions; no mine ventilation network	Jets up to approximately 5 m; fragments over 30 m; a secondary gas explosion in one test	Release geometry and timing require reassessment for mining installations
Dubaniewicz [24]	39 NMC811 cells; 3.2 Ah per cell; 13S3P; 100% SOC	240 W disk heater contacting multiple cells	Modified MSHA-approved XP enclosure; test-container airflow approximately 0.2 m/s	Jet flames escaped the cover joint; the joint and bottom plate deformed	Demonstrates containment failure for the tested assembly and loading conditions

ARC: accelerating rate calorimetry. SOC: state of charge. LEL/UEL: lower/upper explosion limit. MSHA: Mine Safety and Health Administration; XP: explosion-proof. Pressure values are absolute. Reported observations and calculations apply to the specified test conditions.

4.2. Intra-Pack Propagation and Scale Amplification

Whether thermal runaway in a single cell propagates through an entire battery pack depends on whether the energy transferred to adjacent cells exceeds their thermal-stability threshold. Propagation can occur through conductive heat transfer between cell

casings, impingement by hot vent gases, flame radiation, heat conduction through busbars, and electrical connections. The relative contribution of each pathway varies with cell format, pack arrangement, and venting direction [51]. Tests on large-format pouch-cell modules have shown that only a fraction of the energy released by the initiating cell may be sufficient to trigger adjacent cells. Under localised side heating, the onset temperature for failure may also be lower than that measured during uniform heating [52]. Increasing the state of charge raises the releasable energy and generally shortens the interval between successive cell failures. A lower state of charge, however, does not guarantee that propagation will stop. When cells are closely spaced, initially warm, or poorly cooled, gradual heat accumulation may still trigger subsequent failures [53,54].

Electrical configuration and structural layout jointly modify propagation. Lamb et al. [51] observed no module-wide propagation in a 10S1P cylindrical-cell assembly, whereas a 1S10P assembly underwent an energetic failure involving the module. In their stacked pouch-cell assemblies, propagation occurred within 60–80 s in both series and parallel configurations. The contrast indicates that electrical connectivity can influence failure development, but strong thermal contact can dominate the outcome. Initiation conditions also matter. Penetration tests on LFP cells showed that SOC and penetration position affected the thermal response and the likelihood of runaway [55]. Within a pack, wiring passages, cooling gaps, and shared vent channels can carry hot gases past solid barriers. Propagation assessment therefore needs to retain electrical topology, contact geometry, initiation conditions, and internal discharge paths [51,54].

Cell-to-cell propagation and ignition of external vent gases are separate endpoints. Thermal runaway can continue without atmospheric oxygen, while subsequent combustion of released fuel involves the surrounding oxidising atmosphere [23]. Contact heating, conduction through connections and energy carried by hot vent gases can therefore remain relevant when sustained external flaming is absent [51,52]. Propagation assessment should record the cell-failure sequence and the ignition state of the release on a common time basis, distinguishing these heat-transfer pathways from gas-phase combustion. Controlled-atmosphere comparisons, discussed in Section 8.4, provide a means of examining their relative contributions.

Scale amplification changes the release history as well as the total inventory. A pack scenario requires the number of failing cells and the intervals between their failures to be linked to propagation evidence [21,51]. Gas-yield normalisation must retain electrical topology and stored energy: a series string retains the Ah capacity of an individual cell while its higher voltage increases the stored energy, so pack Ah alone can misrepresent the involved cell inventory [23]. Confinement then modifies the release through gas retention, heat transfer, phase changes and flow resistance. The source passed to a roadway model must consequently describe discharge from the enclosure outlet, including its duration, composition, temperature and direction, with external combustion characterised separately. Studies reporting only total gas volume or peak enclosure pressure provide inventory or loading information; a transient outlet source additionally requires time-resolved discharge data.

4.3. Balancing Flameproof Containment, Pressure Resistance, and Controlled Venting

Flameproof enclosure protection addresses the construction and testing of equipment intended for explosive gas atmospheres [56]. For a battery installation, the relevant assessment must establish whether the cell inventory, free volume, discharge paths and thermal-runaway loading are represented by the qualified assembly and its test conditions. Battery failure introduces gas generation, heat transfer, particle ejection and potentially repeated releases from several cells [23,24]. These processes require comparison with the enclosure's demonstrated protection envelope.

Containment can limit direct flame and hot-particle transmission, while restricted discharge can retain heat and generated gases. The design question is whether the available free volume, structure and vent paths accommodate the battery-failure loading while maintaining the flameproof function [22–24]. Pressure, temperature and discharge histories are therefore relevant alongside their peak values. Increasing enclosure tightness alone does not establish this combined performance.

The sealed-cell and pressure-relieving pouch-cell tests in Table 4 illustrate how confinement, thermal contact and discharge behaviour reshape the measured pressure [23]. These results cannot be interpreted as a pressure–capacity scaling relationship. At assembly scale, the modified MSHA-approved enclosure test in Ref. [24] produced jet flames through the cover joint and deformation of the joint and bottom plate. The observation establishes loss of containment for that configuration and loading, while demonstrating the importance of evaluating joint integrity and thermal deformation at enclosure scale. Figure 4 summarises the coupled development of heat, gas and pressure and the possible discharge pathways.

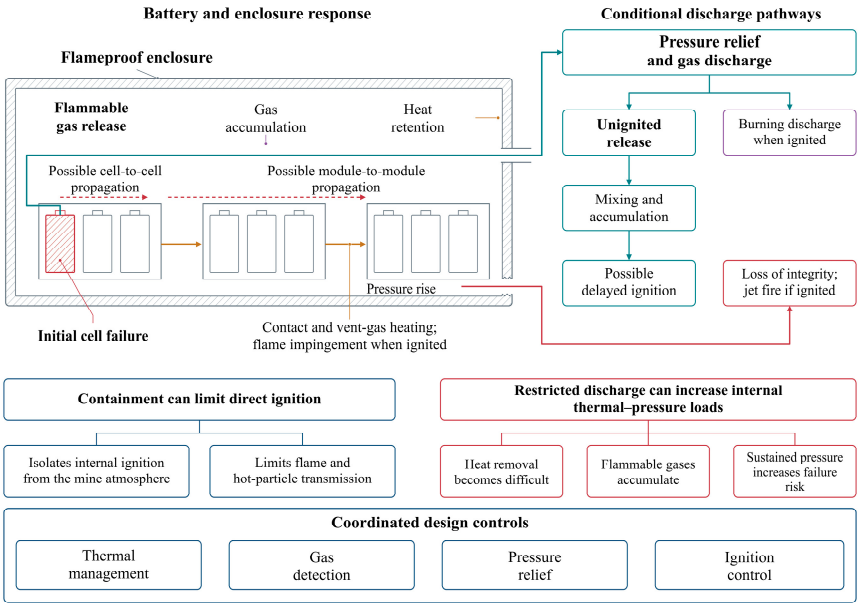


Figure 4. Coupled propagation, heat retention, gas generation and pressure development within a battery enclosure. Discharge may occur as burning jets or unignited gases; external mixing and delayed ignition depend on outlet conditions and the surrounding ventilation. The pathways are conceptual and do not prescribe a fixed event sequence.

Controlled venting requires the opening pressure, discharge capacity, flame-arresting function, blockage resistance and outlet direction to be evaluated together. Relief should occur before damaging deformation, while remaining consistent with normal pressure variations and the assembly's sealing requirements. Electrolyte condensate and entrained debris introduce potential restrictions that require assessment under representative discharge conditions. Outlet performance should be characterised through internal pressure and temperature histories, flame or particle transmission, and the properties of the discharged gases [23,24,46].

External exposure remains relevant even when pressure relief is effective. Unburned gases released through an outlet can mix with roadway air and undergo delayed ignition [26,45]. Outlet placement must therefore be assessed against personnel locations, escape routes, nearby combustible components and the local ventilation field. The enclosure boundary links internal containment to the external source: successful relief must be

evaluated together with the subsequent dispersion and ignition scenarios considered in Section 5.

5. Mine-Type-Dependent Fire and Explosion Hazards

Battery failure can develop through sustained combustion or through the release and accumulation of unignited gases and electrolyte vapour. Both pathways are relevant to coal and metal/non-metal mines. The surrounding atmosphere determines whether battery-derived fuels act alone or interact with methane and combustible dust. Section 5.1 considers vent-gas cloud formation and ignition, followed by methane coupling in gassy coal mines. Section 5.2 examines coal-dust involvement, while Section 5.3 addresses confinement and secondary fire development.

5.1. Vent-Gas Accumulation, Delayed Ignition, and Methane Coupling

Thermal runaway can release combustible gases and electrolyte vapour without sustained external flaming. The discharge contains hydrogen, carbon monoxide, hydrocarbons, and diluting components, with proportions that change with chemistry, SOC, and the stage of failure [26,57]. Amano et al. [45] measured emissions from NMC pouch cells and calculated mixture explosion limits of approximately 7–31 vol% using the measured composition and constituent limits. These values describe the analysed mixtures rather than fixed limits for underground mines. Cloud formation depends on the release history, available air, enclosure and vehicle geometry, and the rate at which ventilation removes the discharge.

Wang et al. investigated collected thermal-runaway gases from five cell chemistries, including LFP and NMC, using a 1 L explosion sphere at 298 K and an initial absolute pressure of 101 kPa [57]. The sampled LFP gases presented greater fire and explosion hazards than the NMC gases in that comparison. This finding concerns the combustion characteristics of released mixtures and addresses a different endpoint from the sealed-cell pressure measurements discussed in Section 4.1 [23]. Chemistry comparisons must therefore distinguish resistance to thermal-runaway initiation, internal enclosure loading and the combustion behaviour of discharged gases. A favourable result for one endpoint alone does not establish the overall safety of a mining-vehicle battery.

Adding methane changes the fuel composition and oxygen balance of a battery-derived mixture. Wang et al. investigated LFP battery thermal runaway in a sealed explosion-proof chamber over methane concentrations of 0–12% and SOC values of 25–100% [58]. Within these conditions, explosion severity peaked at methane concentrations of 4–6%. Their gas analyses associated higher SOC with increased hydrogen and hydrocarbon release, while methane concentrations above 8% produced oxygen-deficient combustion with increased CO and reduced CO_2 formation. Pressure development and CO formation therefore require separate evaluation. The methane concentration associated with the strongest pressure response remains specific to the tested battery, mixture and confinement conditions; it does not define a universal worst-case concentration for mine roadways.

Before ignition, cell reactions and heat transfer within the pack can continue while unburned products enter the enclosure, vehicle compartments, or roadway. A sealed compartment can retain the discharge, whereas restricted openings and longitudinal airflow create non-uniform mixing outside it. Electrolyte vapour and entrained droplets can also change phase as the release cools. The resulting cloud therefore cannot be represented solely by the visible-smoke layer or by a prescribed fire heat-release rate. Its extent depends on the balance between continued release, mixing and removal.

A roadway cloud assessment requires the time-dependent local fuel composition and concentration, oxygen availability and temperature. A spatially averaged concentration

cannot establish the absence of ignitable pockets around the vehicle or within poorly ventilated recesses. Ignition consequences must be evaluated against the mixture present at the assumed ignition location and time, rather than the total gas inventory alone. Where release histories, mixing conditions or ignition timing are unavailable, these quantities should be identified as scenario assumptions and varied explicitly when interpreting the possible extent and severity of delayed ignition.

Ignition may occur at a hot cell casing, electrical fault, incandescent particle, or another source encountered by the dispersed mixture [21,26,46]. A longer release-to-ignition interval can increase the accumulated inventory when removal is insufficient, although the severity of ignition also depends on mixture distribution, oxygen availability and confinement. Methane adds a further fuel contribution in gassy coal mines; it is not required for battery-derived gases to form an ignitable atmosphere. Monitoring and modelling therefore need to address both burning releases and unignited fuel clouds.

5.2. Gas–Solid Hybrid Explosions Involving Coal Dust in Underground Coal Mines

Coal-dust involvement requires a combustible dust fraction to become suspended in a region reached by an ignition source or propagating flame [59,60]. Dust already present in the air and dust newly entrained from deposits represent different fuel-supply conditions. For a battery incident, mobilisation by a venting jet or an initial pressure event is a proposed escalation mechanism whose significance depends on deposit loading, particle properties and the local jet or pressure-wave conditions. Establishing a sequence of vent-gas ignition, dust lifting and subsequent dust combustion therefore requires evidence of entrainment and ignition under the relevant conditions. The presence of deposited coal dust alone does not establish the airborne fuel inventory available for an escalating explosion.

For methane–coal-dust mixtures, the separate gas and dust explosion limits do not fully describe joint ignitability. Amyotte et al. showed that methane below its individual lower explosion limit can increase coal-dust ignitability and reduce the dust concentration needed for flame propagation [61]. Addai et al. examined gas–dust limits in a 20 L vessel [62], three-component mixtures of corn starch, methane and acetone vapour [63], and multiphase combinations involving brown coal or lycopodium, methane or hydrogen, and alcohol sprays [64]. These studies demonstrate interactions among combustible phases, including ignition below individual-component limits. The resulting explosion regime also depends on fuel proportions, ignition conditions and reaction characteristics [65,66]. Battery vent gases and electrolyte vapour introduce different compositions and phase behaviour. Conventional hybrid-mixture tests therefore provide mechanistic support for their possible interaction with methane and coal dust, while battery-containing mixture limits require evidence for the actual constituents and conditions.

The severity of a hybrid explosion depends on coal-dust concentration, particle size, volatile content, methane concentration, ignition energy, and turbulence intensity. Fine particles have a larger specific surface area and generally heat more rapidly, release volatiles sooner, and participate more readily in combustion. At excessively high dust concentrations, however, oxygen depletion, radiative shielding, and particle agglomeration may reduce the effective extent of reaction [59]. Ajrash et al. used a 30 m-long, 0.5 m-diameter tube with an approximately 1 m^3 fuelled section and chemical ignition energies of 1, 5 and 10 kJ [67]. For a mixture containing 6% methane and 30 g/m^3 coal dust, the reported overpressure increased from approximately 0.6 to 1.2 bar as ignition energy increased from 1 to 10 kJ. The pressure-wave and flame responses therefore depended on the initiation conditions as well as the fuel mixture. Wang et al. likewise found that the coal-dust concentration associated with maximum pressure changed with methane concentration [68]. These results establish condition-dependent interactions in conventional methane–coal-

dust systems. Their use in a battery-initiated roadway scenario additionally requires justification of the ignition source, entrained dust inventory and evolving gas composition.

Battery-ejected particles and electrolyte droplets require separate characterisation when assessing multiphase escalation [21,46]. Hot fragments may provide ignition sources, while the contribution of carbonaceous ejecta as a reactive dust depends on particle size, temperature, combustible fraction and concentration. Electrolyte droplets may add vapour through evaporation, with the contribution governed by their composition and thermal history. The conventional gas–dust and spray-mixture studies discussed above do not establish explosion parameters for the simultaneous combination of battery vent gases, methane, coal dust and electrolyte aerosols [62–64]. For roadway scenarios, the available coal-dust inventory should be based on deposit loading and entrainment evidence, accounting for cleaning history, moisture and inert material. Uncharacterised battery ejecta and droplets should remain explicit uncertainties in the scenario rather than being assigned conventional coal-dust parameters.

5.3. Ignition and Cascading Escalation Under Roadway Confinement

Underground roadways impose strong geometric constraints on flame propagation and pressure development. When battery vent gases flow through narrow spaces between a vehicle and the roadway wall, within a charging chamber, or around other equipment, obstacles such as vehicles, supports, and pipelines generate turbulence and flame wrinkling. These effects may accelerate combustion. Reflections of pressure waves from roadway ends, bends, and changes in cross-section can further amplify local pressures [60,69]. The ignition location also affects flame-travel distance and pressure development. Ignition inside a battery enclosure may produce a high-velocity flame and venting jet. Ignition within a vehicle equipment compartment can spread the incident to cables, tyres, and hydraulic systems. By contrast, delayed ignition in the roadway may involve a much larger volume of premixed gases [26,69]. Henriksen et al. measured explosion pressure, pressure-rise rate and explosion limits for three organic carbonates used in battery electrolytes in a 20 L sphere at 373 K and an initial absolute pressure of 100 kPa [70]. These measurements characterise the selected solvent–air mixtures under the stated conditions. Application to battery effluents additionally requires the local temperature, gas composition and vapour fraction to be established, including the effects of dilution and phase changes during discharge and mixing.

Mixing with fresh ventilation air can create new ignitable regions after an earlier burning phase has weakened, provided that unreacted fuel remains or release continues [21,26]. Secondary vehicle fuels, including tyres, hydraulic oil, cables and polymeric materials, may sustain a fire beyond the initial battery release. Vehicle-fire studies can inform the resulting heat and smoke exposure, while the transition from a particular battery discharge to ignition of those fuels requires assessment of the thermal exposure and fuel configuration [7,71]. A sustained secondary fire may in turn continue to heat unaffected battery modules and nearby equipment.

Figure 5 illustrates a conditional escalation scenario for a gassy coal-mine roadway. Battery-derived gas ignition, methane coupling and coal-dust involvement are distinct processes whose occurrence depends on the mixture, ignition and entrainment conditions. Pressure-wave propagation and toxic-product transport can extend the consequences beyond the initial burning region through different mechanisms.

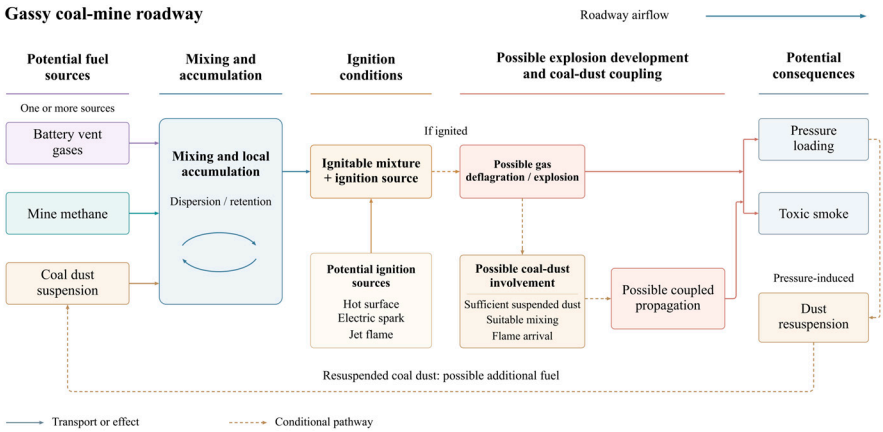


Figure 5. Conceptual escalation pathways in a gassy coal-mine roadway. Battery vent gases may ignite independently or interact with methane and suspended or resuspended coal dust. Hybrid propagation depends on the resulting mixture and ignition conditions; the diagram does not imply that all fuel sources participate in every event.

Table 5 distinguishes the conditions that activate each escalation route and the evidence needed to assess it. For an unignited release, the relevant roadway input is the transient outlet discharge and its composition. Following ignition, combustion heat and product formation become additional source terms, while rapid pressure development requires an appropriate explosion analysis. Coal-dust participation further requires an established suspended or dynamically entrained fuel inventory. Mine type determines which additional fuels and confinement conditions apply; the absence of methane or coal dust does not remove the battery-derived gas-cloud pathway. A mine-specific assessment should identify the supported source data and the assumptions introduced for each transition before transferring the resulting loads to roadway or ventilation models.

Table 5. Representative escalation scenarios, enabling conditions and evidence applicability across underground mine environments.

Scenario	Fuel or Hazard	Ignition Condition	Required Escalation Condition	Possible Outcome	Evidence and Applicability
Delayed vent-gas ignition—general underground mines	Battery gases and electrolyte vapour	Ignition source encounters an ignitable cloud	Local fuel–air mixing; insufficient removal before ignition	Deflagration; pressure loading	Mixture tests/calculations [26,45,57]; roadway cloud formation is scenario-dependent
Vent gas–methane explosion—gassy coal mines	Battery-derived fuels and methane	Ignition of the combined mixture	Suitable fuel–oxygen balance; local confinement	Overpressure; flame spread	Sealed-chamber results [58]; roadway loading requires justified transfer
Gas–dust hybrid explosion—primarily coal mines	Suspended coal dust with combustible gases or vapour	Flame or another effective ignition source	Sufficient suspended or entrained dust; ignitable mixture	Flame acceleration; secondary explosion	Conventional hybrid-mixture tests [61–64,67,68]; battery-containing mixtures require validation
Enclosure failure—general underground mines	Generated gas, retained heat and internal pressure	External ignition is not required for thermal-runaway gas loading	Inadequate discharge capacity or loss of structural integrity	Gas release; jet fire if ignited	Configuration-specific enclosure tests [23,24]

Vehicle-fire escalation—general underground mines	Tyres, cables, hydraulic fluids and polymers	Sufficient thermal exposure from burning battery effluents	Ignition and sustained burning of secondary fuels	Prolonged fire; heat and smoke exposure	Vehicle-fire consequence evidence [7,71]; the battery-to-secondary-fuel ignition link is scenario-dependent
Roadway propagation—mine- and fuel-dependent	Flammable gas or hybrid-mixture regions	Propagating flame or distributed ignition	Suitable mixture distribution; confinement and obstacles	Flame spread; transient pressure loading	Obstacle/tube evidence [60,67]; underground-geometry synthesis [69]

The scenarios constitute an author-proposed classification. Citations identify support for particular mechanisms or tested configurations and do not imply validation of the complete battery-to-roadway accident sequence.

6. Fire-Smoke Transport Through Mine Roadways and Ventilation Networks

Unlike methane- and coal-dust-coupled explosions, smoke transport through confined roadways is relevant to all underground mines. In coal mines, ventilation response must also maintain methane dilution and limit coal-dust involvement. In metal and non-metal mines without a persistent flammable-gas hazard, the priorities shift towards heat and smoke removal, toxic exposure, visibility, evacuation, and access for rescue. The applicable ventilation strategy must therefore reflect both the battery-fire source term and the mine-specific atmospheric hazards.

6.1. Fire Plumes, Ceiling Jets, and Smoke Stratification in Roadways

After a mining vehicle catches fire, buoyant hot gases rise and impinge on the roadway roof. They then spread longitudinally and form a hot, low-density smoke layer in the upper part of the roadway. The stability of this layer is governed by the heat release rate, roadway height, longitudinal airflow velocity, wall roughness, and flow disturbance caused by the vehicle. During the early stage of a fire, heat absorption by the surrounding surfaces reduces smoke temperature and buoyancy. As the rock walls and support structures warm, the heat loss per unit length decreases, allowing smoke to travel farther. Turbulence generated by rough rock surfaces, cables, pipes, and support elements can disrupt the stratified interface and gradually promote mixing across the full roadway section [71,72]. Intermittent venting and multi-peaked heat release from the battery pack also cause repeated variations in plume strength. A single steady-state heat release rate can therefore describe only the overall trend.

Mine-drift stratification studies and generic tunnel blockage studies provide evidence under different configurations. Hansen used data from full-scale underground mining-vehicle fire experiments, together with temperature correlations and numerical modelling, to examine the influence of surface roughness, surface material and the vehicle [71]. The shorter distance to non-stratified conditions predicted for a mine than for a tunnel is a model result under the examined conditions. Lee and Tsai investigated vehicular blockage through small-scale tunnel experiments and numerical simulations, showing that blockage and its position relative to the fire affect smoke behaviour and critical ventilation velocity [73]. Quantitative application to mining vehicles consequently requires the roadway geometry, surface conditions, blockage and source location to be retained.

For a mining-battery scenario, a pack mounted beneath or alongside the vehicle may discharge towards the vehicle body or roadway wall. Outlet location, direction and momentum therefore need to be represented when assessing asymmetric thermal and contaminant exposure around the vehicle.

Smoke stratification does not ensure that the lower part of a roadway remains tenable. CO, HF, and other irritant gases can penetrate below the smoke layer through turbulent

mixing and molecular diffusion. Smoke particles produced by burning vehicle materials may also cause a rapid loss of visibility [74]. Smoke-layer height, temperature, and toxicant concentration do not change synchronously. The vertical position and decay rate of CO stratification may differ markedly from those of thermal stratification. Personnel may therefore be exposed to hazardous toxic-gas concentrations or poor visibility while the thermal conditions remain tolerable [75]. Assessing roadway tenability from visible-smoke-layer height or roof temperature alone may overestimate the available safe egress time.

6.2. Longitudinal Ventilation, Smoke Backlayering, and Fire-Induced Pressure

Longitudinal ventilation transports smoke towards the return side of a roadway, while plume buoyancy can drive part of the smoke upstream along the roof. When the longitudinal airflow is insufficient to overcome this buoyancy-driven counterflow, a backlayering region develops upstream of the fire. The airflow velocity required to prevent sustained backlayering is commonly termed the critical velocity. It is governed mainly by the heat release rate, roadway cross-section, and roadway inclination [73,76–78]. For relatively small fires, the critical velocity increases with heat release rate. Beyond a certain fire size, however, the influence of further increases in heat release becomes less pronounced. The output of a mining-vehicle battery fire changes as thermal runaway propagates and vehicle materials become involved. An airflow velocity that controls smoke during the initial stage may therefore become inadequate as the fire develops. Control of smoke backlayering is an endpoint for a burning release under specified source and ventilation conditions. It does not establish the removal of toxic species, the absence of ignitable gas pockets or the tenability of an escape route. An unignited battery discharge requires a separate assessment of transient release, local mixing and fuel accumulation within the same roadway and ventilation configuration.

Backlayering length provides a more useful measure of the area affected upstream than a simple indication of whether backlayering occurs. Below the critical velocity, increasing the longitudinal airflow generally shortens the backlayering distance. This relationship is modified by the fire location, vehicle blockage, and roadway inclination [79]. A vehicle with a large cross-sectional area reduces the effective ventilation area between the vehicle and the roadway walls. The resulting high-velocity flow may suppress smoke movement on one side of the vehicle while producing a low-velocity recirculation zone behind it. In an inclined haulage roadway, thermal buoyancy also acts along the slope. Smoke naturally tends to move uphill. When mechanical ventilation opposes this buoyant flow, the airflow is more likely to weaken, stagnate, or reverse. When the two act in the same direction, smoke velocity and the extent of downstream contamination may increase substantially [80].

Heating of the air by a fire creates density differences and generates fire-induced pressure. Thermal expansion, increased roadway resistance, and flow restriction near the fire also alter the pre-fire airflow distribution. In a downward-ventilated heated branch, thermally induced pressure can oppose the pre-fire flow. Whether the branch stagnates or reverses depends on the pressure balance in its connected ventilation circuit, including fan pressure, natural ventilation and branch resistances. The relevant comparison is with the available driving pressure across the affected branch, rather than the nominal pressure of the main fan alone. Experiments by Zhou and Wang showed that, following airflow reversal in a downward-ventilated mine fire, partially burned fuel gases may mix with re-entering air and produce a backdraft process distinct from that in a conventional enclosure [81]. Experiments and mine-network simulations by Hu et al. likewise showed that increasing fire intensity raises fire-induced pressure and reduces the original airflow.

Branches with relatively weak ventilation pressure are the most susceptible to smoke reversal [82].

Increasing ventilation flow does not necessarily reduce the overall consequences of an incident. A higher airflow can control upstream smoke movement, but it also supplies more oxygen to the fire. This may accelerate the burning of combustible vehicle materials and transport smoke and toxic products more rapidly towards the return side. A lower airflow may limit some external combustion, yet it can intensify local heating, oxygen deficiency, incomplete combustion, and smoke accumulation. Once initiated, some thermal-runaway reactions within a battery do not depend on the external oxygen supply. Reducing the ventilation flow therefore cannot immediately stop heat and gas generation within the cells. Ventilation control should not aim simply to maximise or minimise airflow. It must balance the need to limit fire growth, preserve viable evacuation directions, and prevent smoke from entering critical working areas.

6.3. Airflow Redistribution and Long-Range Contamination in Ventilation Networks

An underground mine contains a complex ventilation network formed by intake and return airways, crosscuts, declines, working faces, and chambers. During a fire, changes in air density, local resistance, and pressure within the heated branch alter the original airflow distribution. Smoke may then pass through intersections and enter areas that are not directly connected to the fire source. Figure 6 links ceiling-jet transport, smoke backlayering, and stratification breakdown near the fire to local recirculation, airflow splitting, and cross-area dispersion within a branching network. The smoke hazard consequently shifts from longitudinal transport along a single roadway to uneven distribution among multiple branches. Smoke partitioning at an intersection is governed by the airflow rate, cross-sectional area, turning resistance, branch angle, and geometry of each connected roadway. Ceiling-jet separation and asymmetric smoke distribution may also occur at bifurcations. The proportion of smoke entering each branch therefore cannot be determined solely from its cross-sectional area [83,84].

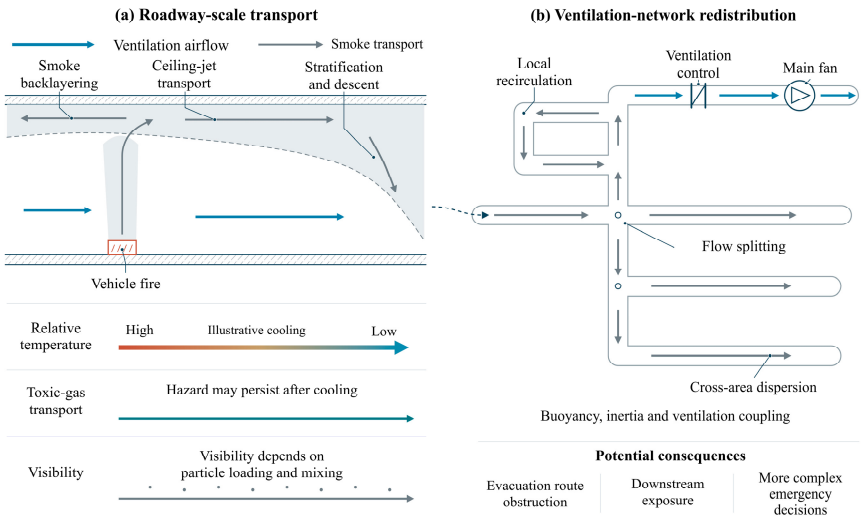


Figure 6. Transport of heat, smoke and toxic gases from a mining-vehicle fire through roadways and a branching ventilation network. Downstream exposure depends on dilution, leakage, mixing and airflow redistribution; the schematic does not prescribe a concentration gradient.

Continuous operation of the main mine fan does not guarantee that every local branch will retain its original airflow direction. As resistance increases in the fire-affected branch, parallel branches may carry a larger proportion of the total airflow, while weakly

ventilated zones near the fire may experience stagnation or reversal. Simulations of fires in branching roadways further show that, when smoke from a side branch enters a main roadway, its backlayering length and the airflow required for control depend on the side-branch flow rate, the main-roadway velocity, and the location of the junction. Critical-velocity relationships developed for a single roadway cannot therefore be applied directly to a branching network [85]. Fire-induced pressure often has its greatest effect not in the main airway carrying the highest flow, but in parts of the network where the mechanical ventilation pressure differential is small [82]. If the affected vehicle is located in a decline, crosscut, or major intersection, smoke may enter several mining districts at once. If it is located in a stable return-air branch, the direction of contamination is more predictable. The network position of the source therefore determines which branches and occupied areas can receive contaminated airflow. Its influence must be evaluated together with the release history and ventilation state within the particular network; junction-flow studies alone do not establish a general ranking between source location, battery capacity and fire intensity.

Smoke temperature and toxicant concentration follow different transport processes. Heat is transferred to roadway surfaces, while gas concentrations depend on release rate, dilution, leakage, mixing and any species-specific losses. Hazardous exposure can therefore persist after substantial cooling, but concentration need not increase with downstream distance [86,87]. Local accumulation and fresh-air inflow can produce markedly different concentration histories in neighbouring branches.

A roadway source should describe the material and energy entering the modelled domain after enclosure retention, discharge and any upstream combustion. A burning-release scenario requires the external combustion heat-release history and the relevant combustion-product and smoke-production rates. An unignited-release scenario requires gas and vapour mass-flow histories, composition, temperature and outlet geometry, direction and momentum. Internal reaction heat and abuse-heater energy may reach the roadway through hot discharge or heated surfaces, but their contribution must be accounted for separately to avoid double counting with an external combustion source.

All source histories should use an explicitly defined event clock and consistent mass or volume bases. Resampling and conversion of the source data should preserve the combustion energy and discharged species inventory over the same interval:

$$E_{comb} = \int_{t_0}^{t_1} \dot{Q}_{comb}(t)dt \quad (2)$$

$$M_{i,out} = \int_{t_0}^{t_1} \dot{m}_{i,out}(t)dt \quad (3)$$

Here, E_{comb} is the total external combustion energy released over the integration interval, and $\dot{Q}_{comb}$ is the corresponding time-dependent heat-release rate. $M_{i,out}$ is the total mass of species i discharged through the outlet, and $\dot{m}_{i,out}$ is its outlet mass-flow rate. The times t_0 and t_1 bound the common integration interval. These integral checks constrain the represented energy and inventory; peak rates, pulse durations and release timing also require examination at the resolution relevant to the predicted endpoint. A release history reconstructed from total gas volume alone remains a scenario assumption.

Yuan et al. [86] demonstrated source-history transfer using a diesel fire in the Safety Research Coal Mine operated by the National Institute for Occupational Safety and Health (NIOSH). The test burned 5.7 L of diesel in a 0.6 m × 0.6 m pan, with a measured pre-fire inlet velocity of 0.71 m/s. The Fire Dynamics Simulator (FDS) represented the first 400 m of the transport route and was calibrated against CO measurements. A modified MFIRE implementation then received the FDS-generated dynamic heat-release history, with network resistances and fan characteristics obtained from a ventilation survey. Compared with a fixed source of approximately 500 kW, the dynamic input reproduced the changing

CO profile more closely. Residual downstream differences remained sensitive to resistance and leakage representation. This was a transfer of a fire-source history into a network model, rather than a demonstrated exchange of all battery-release variables.

Zhou et al. [87] evaluated MFIRE against full-scale diesel and conveyor-belt fire tests. They reconstructed heat-release histories from measured fuel mass loss and fuel heat of combustion, and represented fire development using idealised time-dependent curves. Their HRR-linked CO source followed

$$\dot{V}_{CO}(t) = \beta \dot{Q}_{comb}(t) \tag{4}$$

where β denotes the CO volume produced per unit combustion heat, using consistent units and volume-reference conditions. The CO production constants were adjusted against measured concentrations. Agreement with these data therefore includes calibration and remains specific to the tested fuels and ventilation conditions.

For battery incidents, negligible external combustion heat release does not establish negligible CO or other gas release. An unignited discharge requires an independently specified gas-generation and outlet-release history. Deriving its contaminant source solely from combustion HRR would omit the non-flaming pathway, while adopting a diesel or conveyor-belt CO production constant would require separate justification.

Where a locally resolved computational fluid dynamics (CFD) model is connected to a ventilation-network representation, the interface should preserve transported mass and species fluxes. For an outward-flowing part of a cross-section, the advective gas-species transfer is

$$\dot{m}_{i,CFD\to net}(t) = \int_{A_{out}(t)} \rho Y_i(\boldsymbol{u}\cdot\boldsymbol{n})dA \tag{5}$$

and its corresponding mass-flow-weighted species mass fraction is

$$\bar{Y}_{i,out}(t) = \frac{\int_{A_{out}(t)} \rho Y_i(\boldsymbol{u}\cdot\boldsymbol{n})dA}{\int_{A_{out}(t)} \rho(\boldsymbol{u}\cdot\boldsymbol{n})dA} \tag{6}$$

Here, A_{out} is the portion with outward flow, ρ is gas density, Y_i is the species mass fraction, $\mathbf{u}$ is velocity, and $\mathbf{n}$ is the outward unit normal. The average is defined only when outward mass flow is non-zero; opposing inflow should be accounted for separately. These expressions describe advective gas transport, with additional diffusive contributions retained where significant. Mass fractions, volume fractions and ppm values require consistent conversion before transfer.

Thermal exchange should preserve transported sensible enthalpy on an agreed reference basis and specify which heat losses are represented in each model. Combustion HRR at the source is not identical to the thermal flux crossing a downstream section. A network representation using mixed branch concentrations also cannot retain the local peaks within a vent jet, vehicle wake or stratified layer. The complete-mixing assumption discussed by Zhou et al. [87] illustrates why agreement with branch-scale CO transport does not establish local exposure accuracy. If network changes alter the airflow supplied to a CFD region, compatible boundary conditions must be updated rather than assuming that a previously calculated local solution remains applicable.

Directional discharge can be represented when outlet geometry, transient mass flow, temperature, composition and momentum are specified and adequately resolved. Compressible jet expansion and rapid explosion-pressure propagation require formulations that retain the relevant pressure dynamics. Agreement for smoke arrival or CO transport in the fire studies above does not establish that these additional processes are resolved.

Said et al. [88] simulated large-format battery incidents over airflow velocities of 0–3.5 m/s and used heat-release and airflow histories as inputs to deep-learning predictions of temperature, smoke and CO. These results concern the simulated source and transport conditions. Hong et al. [89] generated 1000 numerical mine-tunnel fire scenarios under

varied ventilation, thermal and geometric conditions to develop rapid smoke-movement predictions. For such surrogate models, agreement with numerical cases assesses reproduction of the underlying simulation; applicability to a mining-battery scenario additionally depends on the represented release physics, outlet conditions, blockage and ventilation geometry.

Ventilation adjustments affect smoke movement, gas accumulation, and evacuation routes at the same time. Stopping a local fan, increasing main-fan power, or changing the position of doors and regulators may protect one branch while worsening conditions elsewhere. Short-term airflow reversal may also occur during the adjustment. A fixed response is therefore unlikely to remain effective across different fire locations and stages of development. Decisions should be based on real-time measurements of airflow velocity, pressure differential, temperature, gas concentration, and personnel location. Before any adjustment is implemented, its network-wide effects should be evaluated to confirm that contaminated air will not be redirected towards occupied areas or existing escape routes.

7. Human Tenability, Evacuation, and Mine-Wide Consequences

Tenability during a mining-vehicle fire is governed by temperature, thermal radiation, toxic gases, oxygen depletion, and visibility. CO reduces the oxygen-carrying capacity of blood, while CO_2 stimulates respiration and increases the inhaled dose of other contaminants. A falling oxygen concentration further aggravates hypoxic effects. HF and other fluorinated compounds released from the battery may also mix with smoke produced by burning tyres, cables, and hydraulic fluids. Loss of escape capability depends on contaminant concentration and exposure duration, together with thermal and visual conditions. The available safe egress time (ASET) is the interval from a specified incident origin to the selected tenability limit for the conditions and protection considered. Its estimation requires time-dependent hazard fields and personnel locations, because ventilation and occupant movement determine the exposure encountered [90–92]. Visibility impairment can restrict movement even when the selected thermal and toxic-exposure criteria have not yet been exceeded. By obscuring lighting, signs, and obstacles, smoke reduces walking speed and increases the risk of disorientation, falls, and entry into contaminated branches [93,94]. In a controlled smoke-chamber study involving ten participants, Martell et al. evaluated the detectability of illuminated fibre lifelines and a conventional rope lifeline. Green- and blue-lighted fibres were more readily detected under the tested cap-lamp-off condition, whereas cap-lamp illumination markedly impaired detection [95]. These findings support the potential of illuminated lifelines as visibility aids under specified conditions; their effects on evacuation speed and successful route following were not established by the experiment. Inclined roadways, standing water, rails, pipes, and uneven floors further increase the effects of limited visibility.

Mine-evacuation time includes incident detection, alarm transmission, personnel response, preparation of self-contained self-rescuers, and travel to safety. Battery failure may produce an unignited gas release before visible flames, while subsequent propagation can change the release rate and combustion conditions. Hazardous exposure or flammable accumulation may therefore develop without a strong visible-smoke indication. Waiting for visible flames or confirmation of the full incident scale can delay the response. Changes in airflow and roadway access can also invalidate a previously preferred escape route.

Ventilation-based route studies provide model-based comparisons of travel distance and hazard exposure. Lotero et al. coupled VentSim fire simulations with a minimum-cost network-flow method [96], whereas Bi et al. formulated evacuation planning as a multi-objective constrained shortest-path problem [97]. Xiao et al. examined smoke diffusion and evacuation routes using a complex-network representation of a metal mine [98]. The

resulting route rankings depend on the assumed incident, ventilation state, hazard criteria, and movement parameters. Application to a battery-vehicle incident requires time-dependent source and ventilation conditions, with heat, gas exposure, visibility, and passability checked along each route at the occupants' predicted times of passage. These model comparisons do not by themselves establish escape success probabilities for battery-vehicle incidents.

When correctly activated and worn, self-contained self-rescuers provide breathable air independently of the contaminated ambient atmosphere. For route assessment, usable endurance should be assigned from device-specific performance information under the stated workload and service condition. Correct donning, continuous use, and exposure before effective protection is established require separate consideration. Kowalski-Trakofler et al. interviewed eleven miners, manufacturers, and researchers and identified concerns including unit heat, breathing resistance, and starting procedures [99]. This qualitative evidence supports equipment-specific familiarisation and operating training; it does not provide a general coefficient for converting rated duration into usable escape time. Equipment condition, training, communication, and access to current environmental information also influence self-escape [100]. Respiratory protection does not remove route constraints arising from heat, impaired visibility, physical obstruction, or explosion effects.

Figure 7 places incident development, evacuation, and self-rescuer use on a common time axis. The origin, $t = 0$, is the specified onset of the release or fire scenario and must be used consistently for both hazard development and evacuation. Required safe egress time (RSET) is the elapsed time from this origin until personnel reach a suitable exit or usable refuge, including detection, alarm transmission, response, preparation, and travel. Activities that overlap should not be counted twice.

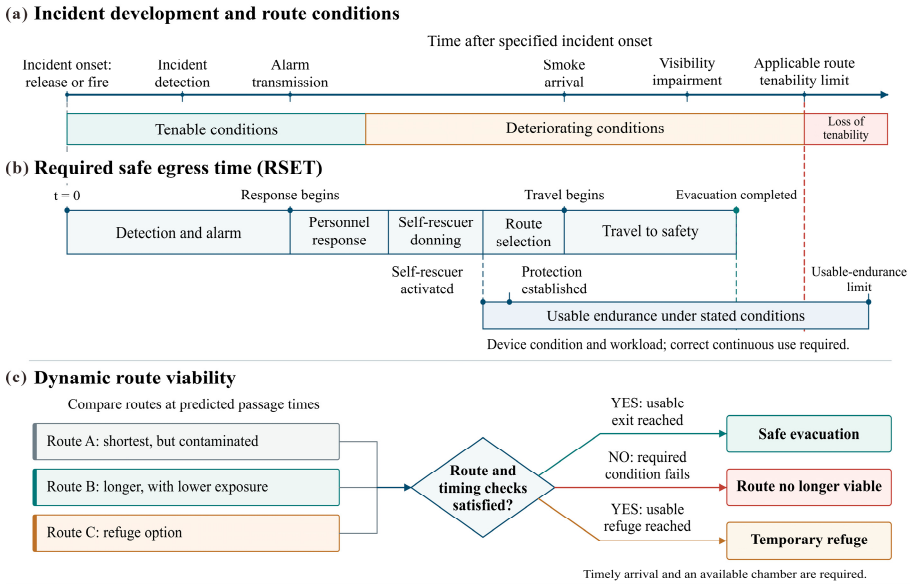


Figure 7. Conceptual timeline linking incident development, evacuation, self-rescuer use, and route viability during a mining-vehicle incident. All event times use the same specified incident origin; self-rescuer endurance is counted from activation. The illustrated case reaches a suitable exit before the applicable route-tenability and endurance limits. A refuge is an alternative destination only if it can be reached in time and provide the required protection. Event order and spacing are illustrative and do not represent measured delays. Based on Refs. [90,92,96,99–101].

For the illustrative route, the completion time, t_{safe}, equals RSET. The two timing checks are: RSET < ASET, $t_{safe} < t_{act} + D_{eff}$. Here, ASET is the applicable route-tenability limit expressed as elapsed time from the same origin; t_{act} is the self-rescuer activation time; and

D_{eff} is the usable endurance assigned to the specific device under the stated workload and operating conditions. The endurance check assumes correct, continuous use after donning. Exposure before effective protection is established, including any interval after activation, must also be assessed. Each route segment should be checked at the predicted passage time for accumulated exposure, heat, visibility, and physical passability. A later deterioration in a segment already traversed does not automatically invalidate the completed passage. The schematic illustrates the timing relationships; predicting escape outcomes additionally requires these route and protection checks.

A refuge chamber may serve as an alternative destination when surface evacuation cannot be completed along a viable route, provided that personnel can reach and enter it before the applicable route and respiratory-protection limits are exceeded. Its suitability depends on accessibility, sealing, breathable-air provision, occupancy, communication, and the internal temperature and humidity expected for the intended duration. Reaching the chamber is therefore only the first stage of assessing refuge protection. Training should address chamber operation and the physiological and psychological demands of prolonged occupancy [100]. Margolis et al. evaluated refuge-chamber expectations training with 336 underground coal miners [101]. Their post-training assessment documented participants' responses and knowledge, but the absence of a pre-training baseline prevented measurement of knowledge gains. This study informs training content and evaluation; it does not quantify the chamber's protective endurance or occupants' survival probability. Following a fire-induced airflow reversal, a chamber normally located on the fresh-air side may also become exposed to contamination. If its entrance lies close to a haulage roadway or the affected vehicle, personnel may be unable to reach it safely. A vehicle fire can damage electrical power, communications, compressed-air services, and ventilation infrastructure, while also obstructing access for rescuers and equipment. Rescue operations must account for residual high voltage, thermal-runaway reignition, explosion of unburned vent gases, and contaminated firefighting runoff. An incident in a return-air branch may have limited effects on other occupied areas if airflow remains directed away from them and alternative escape routes and essential services remain available. An incident in an intake decline, charging chamber, or critical intersection can affect multiple districts when contaminants enter shared intake paths, the incident obstructs a common escape route, or fire and explosion damage shared ventilation, power, or communication infrastructure. Assessment of mine-wide consequences should therefore trace the connections between incident location, contaminant transport, occupied areas, escape routes, and shared services. These connections define the conditions under which a local battery incident can develop into a wider mine emergency.

8. Layered Protection from Battery Systems to Mine Emergency Response

8.1. Fault Prevention, Multi-Parameter Monitoring, and Early Warning

The first priority in the safety design of a battery-electric mining vehicle is to prevent an individual cell from entering thermal runaway. Cell chemistry, manufacturing quality, and consistency in capacity and internal resistance define the initial safety margin. The battery pack must also withstand heavy-duty cycling, sustained vibration, mechanical impact, dust, moisture, and repeated temperature fluctuations. A more thermally stable chemistry can reduce the severity of some abuse reactions, but it cannot eliminate internal short circuits, gas generation, or failure propagation. Battery selection should therefore consider heat and gas release at high states of charge, latent damage after mechanical deformation, and pressure development within a confined enclosure. Excessive energy

concentration in a single sealed compartment should also be avoided through appropriate module segmentation.

Conventional battery management systems monitor cell voltage, current, surface temperature, state of charge, and insulation resistance. These signals are effective for detecting overcharge, overdischarge, overcurrent, and some external short circuits. They may respond too late, however, to an internal micro-short circuit or local mechanical damage. Surface-temperature measurements are particularly limited because the measured value depends on sensor position, thermal contact, and coolant-flow distribution. Local heat generation can continue before a clear change is observed at the pack surface. Monitoring should therefore consider the rate of temperature rise, cell-to-cell temperature differences, voltage deviation, insulation change, cooling-system condition, and recent duty load rather than relying on a single fixed threshold.

Mechanical measurements can complement electrical and thermal monitoring, but their interpretation requires a baseline for normal operation. Yu et al. monitored strain and temperature within a graphite electrode using embedded distributed optical fibre [102], demonstrating access to internal structural changes during cycling. Such measurements require discrimination between normal expansion and fault-related deformation before they can support an alarm. Song et al. used module-space pressure variation associated with venting to warn of thermal runaway under the tested abuse conditions [48]. Transfer of this pressure-based approach requires the module free volume, leakage, venting arrangement, and sensor location to be retained or explicitly reassessed. These methods provide complementary information, with warning performance determined for the intended cell and pack configuration.

Gas and impedance measurements can further extend the warning window. Electrolyte vapour, CO_2, CO, H_2, and characteristic hydrocarbons may be detected before a pronounced surface-temperature rise or the onset of thermal runaway. Liao et al. [47] used C_2H_4, CH_4, and CO to warn of thermal runaway in NMC cells and reported warning times of several minutes at different states of charge. Cui et al. [49] also showed that gas composition and release behaviour depend strongly on battery chemistry and fault conditions. In matched abuse tests, Torres-Castro et al. [50] found that rapid electrochemical impedance spectroscopy (EIS) provided a longer warning interval than volatile organic compound (VOC) sensing during external heating, whereas VOC sensing responded earlier during 1C overcharge. The warning interval also changed with electrical configuration. The tested comparisons show that the ordering of diagnostic signals depends on fault mode and electrical configuration. Warning performance should be reported from the registered alarm to a specified endpoint, such as initial-cell thermal runaway or subsequent propagation. Gas transport to the sensor, sensor response, signal processing, communication, and actuator operation affect the time available for intervention. A precursor interval measured from the onset of release cannot be treated as the installed system's actionable warning margin. Evaluation should also establish whether the detected stage still permits removal of the abuse input, as demonstrated in the intervention tests of Torres-Castro et al. [50]. Complementary signals should be assessed for missed detections, false alarms, and operation when a sensor or communication link is unavailable.

Early warning should trigger actions that remain feasible at the detected stage of failure. Figure 8 presents a three-level response structure proposed in this study for coordinated intervention by the BMS and the battery thermal management system (BTMS). An early anomaly prompts signal assessment and adjustment of cooling or operating load; a developing fault prompts power derating or interruption of charging and discharging. Confirmed venting or rapid deterioration prompts alarm transmission, protection of exposed personnel, electrical isolation where feasible, and emergency cooling where effective access is available. The response may move directly to a higher level without

sequential passage through the preceding levels. Signal cross-checking should not delay an urgent response to a credible escalation indication. High-voltage disconnection reduces external electrical input but does not terminate self-sustaining reactions within a failed cell. The design must therefore establish which monitoring, alarm, and cooling functions remain available after isolation. Laboratory lead times [47–50] inform this structure but do not establish its trigger thresholds or effectiveness in a mining vehicle.

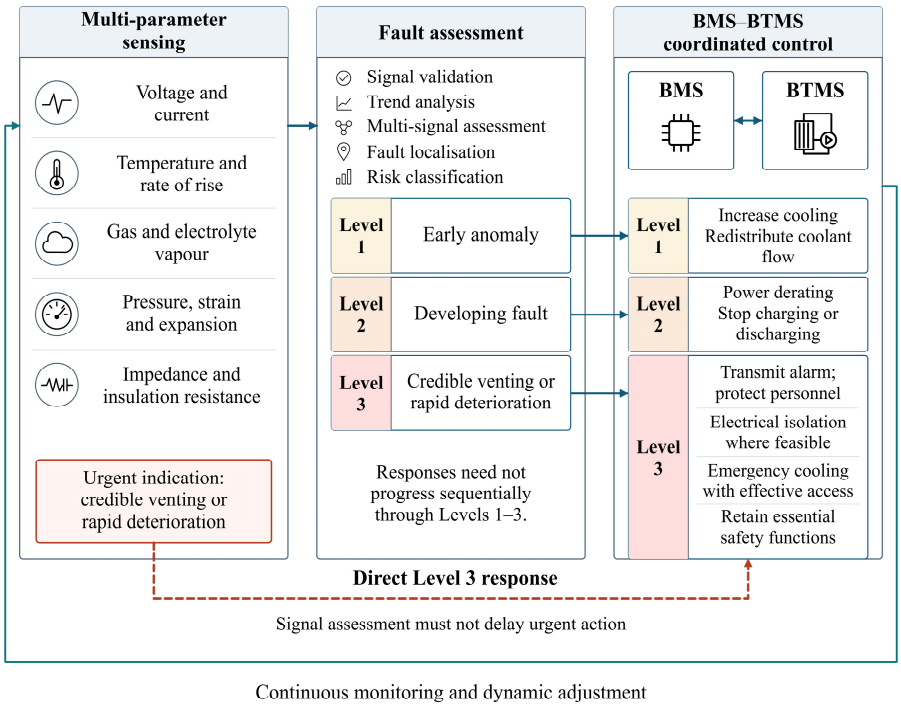


Figure 8. Proposed conceptual integration of multi-parameter sensing, fault assessment, BMS–BTMS control, and graded intervention in a battery-electric mining vehicle. Sensing principles are informed by Refs. [47–50]; intervention thresholds require validation for the intended battery and mining conditions.

Mining conditions impose additional requirements on the monitoring system itself. Dust, high humidity, water exposure, vibration, and repeated mechanical shock can contaminate sensors, cause drift, loosen connections, or obstruct sampling paths. Sensors and communication links therefore require self-diagnostic functions, plausibility checks, redundancy for safety-critical variables, and periodic calibration under representative mine conditions. Vehicles that have experienced collision, water ingress, an insulation alarm, abnormal deformation, or unusual heating should be removed from service for inspection even if they remain operational. Residual capacity alone cannot demonstrate battery health because it does not reveal local mechanical damage, internal-resistance growth, cooling-system degradation, or deteriorating insulation.

8.2. Precision Thermal Management and Prevention of Heat Accumulation

Thermal management in a battery-electric mining vehicle should control both the maximum cell temperature and temperature non-uniformity within the pack. Its safety function is not limited to removing heat during normal operation. It should also prevent local heat accumulation from developing into an irreversible cell failure. A fixed cooling rate may be inadequate during rapid charging, prolonged uphill haulage, or incipient internal faults. The battery management system and battery thermal-management system should therefore operate as coupled safety functions. Changes in temperature-rise rate,

cell-to-cell temperature difference, voltage, pressure, gas concentration, and operating load can be used to adjust cooling capacity, redistribute coolant flow, or reduce vehicle power before thermal runaway begins.

Indirect liquid cooling is a practical option for high-power battery packs, but its performance depends on cell-to-plate contact, thermal-interface resistance, channel arrangement, and coolant-flow distribution. An acceptable average pack temperature may still conceal local hot spots. Immersion cooling reduces these interfacial resistances by placing cells or modules in direct contact with an electrically insulating liquid. Single-phase immersion has been shown to improve temperature uniformity during battery operation [103], while fluorocarbon-based systems have been investigated for enhanced thermal safety [104]. Abuse experiments further suggest that immersion can delay thermal runaway and reduce heat transfer to neighbouring cells under specific conditions [105,106]. Its effectiveness nevertheless depends on the coolant volume, flow rate, thermal properties, and continued contact with the failed cell. Electrical insulation, flash point, chemical stability, toxicity, seal compatibility, and long-term ageing must also be considered. These requirements are especially important when an immersion system is integrated into a flameproof enclosure.

Phase-change materials (PCMs) can absorb short-duration heat peaks through latent heat storage and reduce dependence on continuous pumping. Their capacity is finite, however, and the stored heat must eventually be removed. Conventional organic phase-change materials may also suffer from low thermal conductivity, leakage, and flammability. Microencapsulation confines the phase-change core within a protective shell and improves shape stability. Microencapsulated phase-change-material slurries can additionally act as circulating coolants that transport both sensible and latent heat [107]. Nanoencapsulated inorganic phase-change materials have shown potential for reducing peak temperature and suppressing thermal-runaway development while avoiding some of the flammability associated with paraffin-based materials [108]. Practical application still requires attention to capsule rupture, particle sedimentation, viscosity, thermal cycling, and the added mass and volume of the material.

Hybrid systems can combine the rapid heat absorption of a phase-change material with the continuous heat removal provided by liquid cooling. Experiments have shown that this combination can control temperature accumulation and limit thermal-runaway propagation more effectively than passive phase-change materials alone under the tested conditions [109]. The benefit must be weighed against additional mass, pumping power, sealing requirements, and system complexity. Lower operating temperature, delayed thermal-runaway onset, and interruption of propagation are distinct outcomes. A thermal-management study under normal cycling supports temperature control, while an abuse experiment supports only the failure conditions and configuration actually tested. For mining integration, comparisons should retain coolant inventory, flow, cell contact, initiation power, failed-cell number and the observation period. Vibration, inclination, leakage, dust and maintenance then determine whether the demonstrated thermal function can be sustained in service.

8.3. Lightweight, Mechanically Robust, and Fire-Resistant Pack Integration

The addition of flameproof enclosures, propagation barriers, cooling circuits, immersion liquids, and pressure-relief components increases the mass and volume of a mining-vehicle battery system. These additions reduce the effective specific energy at the vehicle level and may increase energy consumption during repeated acceleration or uphill haulage. Lightweight design is therefore necessary, but mass reduction cannot be pursued independently of impact resistance, enclosure stiffness, fire endurance, and sealing integrity. Structural optimisation, load-path design, and cellular or sandwich structures may reduce

enclosure mass while maintaining energy absorption under mechanical loading. For example, steel–aluminium honeycomb sandwich structures and bio-inspired cellular designs have shown the potential to improve the mass–crashworthiness balance of road-vehicle battery enclosures [110,111]. Their applicability to mining vehicles remains subject to verification under lower-speed but higher-frequency impact, vibration, floor contact, and rock-strike conditions.

Carbon-fibre-reinforced polymers offer high specific stiffness and strength, corrosion resistance, and considerable potential for reducing enclosure mass. Topology optimisation and reinforced composite layouts have been used to produce lightweight battery enclosures with acceptable deformation under selected quasi-static loads [112]. Carbon-fibre composites should not, however, be treated as a direct replacement for a metallic flameproof enclosure. Polymer matrices can soften, decompose, delaminate, or lose load-bearing capacity under thermal-runaway fire exposure. Carbon fibres are also electrically conductive, which introduces additional requirements for insulation, grounding, and electromagnetic compatibility. Sterling et al. [113] used finite-element models driven by representative battery-fire loading to estimate damage and residual strength in a composite enclosure specimen. The predicted strength reductions were approximately 20% for the single-cell loading and 56% for the multi-cell loading considered. These are specimen-level model results, rather than measurements of a complete mining enclosure, but they identify residual load-bearing capacity as a necessary design endpoint.

A hybrid enclosure may provide a more credible route for underground mining applications. Metals can be retained at flameproof joints, threaded connections, pressure-bearing regions, coolant interfaces, and surfaces exposed directly to high-temperature jets. Fibre-reinforced composites or sandwich panels may then be used in secondary covers, external stiffeners, protected wall sections, or non-critical immersion-system components. Fire-resistant coatings, ceramic layers, mica barriers, or intumescent materials can further protect the load-bearing substrate. Bench-scale fire tests have shown that housing materials differ substantially in insulation performance, backside temperature, integrity, and burning behaviour, so a single flammability rating is not sufficient for enclosure selection [114]. Connections between dissimilar materials also require attention because thermal expansion, vibration, moisture, and galvanic corrosion can progressively weaken seals or joints.

Immersion systems, encapsulated phase-change materials, and composite structures are supported by different forms of evidence. Operating-temperature studies establish heat-removal performance; abuse tests examine runaway delay or propagation under selected conditions; structural simulations evaluate deformation or residual strength for prescribed loading. Readiness for a mining installation requires the demonstrated function to be retained in the assembled system under its intended operating and incident conditions.

Integration assessment should explicitly examine the interfaces between these functions. Coolant and barrier inventories affect the remaining gas free volume and available discharge paths. Propagation barriers can alter both heat transfer and the transport of hot gases, while venting arrangements affect pressure retention and external exposure. Electrical isolation may also remove power from pumps, controllers, or communication equipment unless their required operation is supported separately. The assessment should identify shared dependencies and evaluate sensor loss, loss of cooling flow, blocked discharge, and interruption of the relevant power supply. For each case, the required protective function, its duration, and the receiving thermal or gas-release conditions should be specified.

The final design should be evaluated as an integrated structure rather than as separate lightweight, thermal, and flameproof components. Relevant criteria include mass,

usable battery volume, stiffness, impact-energy absorption, fatigue resistance, thermal insulation, flame penetration, pressure resistance, sealing performance, and residual strength after fire. Tests should reproduce representative mechanical loading, thermal-runaway jets, internal pressure, coolant exposure, vibration, dust, and water ingress. Conventional road-vehicle impact tests or small material coupons cannot demonstrate the integrity of a full mining-vehicle enclosure. Qualification should identify the safety functions required in each specified incident state, their performance criteria and required duration, and the measured behaviour of the complete assembled enclosure under the declared test conditions.

8.4. Thermal-Runaway Propagation Control and Incident Mitigation

Propagation control should address conductive heating and hot discharge as well as external flame impingement. Lee et al. tested fully charged 18650 LCO arrays with 5 mm gaps and barriers under nitrogen flow. Ceramic-fibre barriers slowed propagation by more than a factor of 30, but none completely prevented it [115]. Continued failure propagation under these conditions demonstrates that suppression of external flaming alone does not eliminate the transfer of energy to neighbouring cells. The nitrogen barrier tests and air reference tests also used different imposed gas-flow conditions, so their comparison should not be treated as a universal oxygen-dependent propagation multiplier. Increasing cell spacing can reduce conductive coupling, but its effect on packing density and discharge paths must be considered, and an air gap alone may not stop a hot jet. Module segmentation should therefore create relatively independent thermal, pressure, and electrical zones. Partitions must withstand jet impingement and short-duration heating, while cables, busbars, and cooling lines should not form rapid heat-transfer paths across the barriers. Fuses and contactors can reduce external energy input, but they cannot stop the internal reactions of a cell that has already entered thermal runaway.

Venting design should be assessed for both internal pressure control and the conditions of the external release. Distributed outlets and common manifolds alter the paths through which hot gases reach neighbouring modules, personnel, and the roadway. A manifold may direct discharge away from the cab while creating retention or accumulation elsewhere. Vent area, opening pressure, flow resistance, and blockage tolerance should therefore be evaluated against the relevant gas-generation history. Sealed-enclosure experiments demonstrate the dependence of pressure on cell chemistry and free volume [22,23]; they do not establish the performance of a different vented pack configuration. Pressure relief does not remove the toxicity or flammability of an unignited discharge. Flame-arrester performance likewise requires assessment for the intended gas mixture, temperature, flow, and particle or condensate loading. Pack-level evaluation should record pressure together with outlet mass flow, composition, temperature, and release direction, allowing the receiving vehicle and roadway hazards to be assessed.

Road-vehicle and industrial battery standards provide a useful foundation for safety evaluation. UN Regulation No. 100 [116] addresses thermal propagation and occupant warning, while UL 2580 [117] and IEC 62619 [118] include mechanical, electrical, thermal, and abuse testing requirements. However, these requirements do not fully represent the confined operating conditions of underground mines. Battery vent gases, heat, smoke, and toxic effluents are common concerns in both coal and metal/non-metal mines, although the surrounding combustible atmosphere differs between mine types. In gassy coal mines, methane and coal dust introduce additional risks of external ignition and hybrid explosion. Mining battery packs should therefore be assessed for controlled venting, enclosure integrity, pressure-relief performance, and the ability of protective components to remain functional under site-specific dust, moisture, vibration, and gas conditions. A warning period designed for road-vehicle occupants also cannot be treated as the

available safe time for mine personnel because smoke may reach workers elsewhere through the ventilation network.

China has established mine-specific safety requirements for lithium-ion traction batteries used underground.KA 26-2025 [119] entered into force on 1 December 2025 and is listed as an active mandatory industry standard. GB 48146-2026 [120] was issued on 27 August 2026 as a mandatory national standard and is scheduled to take effect on 1 March 2027.. The national standard extends safety requirements across the battery lifecycle and provides a common baseline for coal and metal/non-metal underground mines. Its implementation should be supported by coordinated provisions for safety evaluation and lifecycle management, monitoring and early warning, power-source and enclosure design, charging safety, battery-swapping safety, and emergency response. In coal mines, these provisions must account for methane and coal-dust hazards. In metal and non-metal mines, greater attention may be required for large pack capacity, mechanical impact, water ingress, toxic effluents, confined smoke transport, and evacuation, unless flammable gases or combustible dusts are also present.

Table 6 summarises representative early-warning and mitigation experiments, including prevention of thermal runaway after termination of an abuse input and slowing of propagation without complete arrest. Once thermal runaway begins, cooling and suppression should be evaluated against distinct incident endpoints: extinction of external flames, reduction of cell temperature, interruption of propagation, and control of residual gas release. Water-based agents can remove heat when sufficient liquid reaches the relevant surfaces, but delivery may be limited by enclosure access, jet discharge, or roadway airflow. The performance of water mist and additives depends on droplet delivery, application rate, duration, and the tested battery configuration [121]. Other agents should likewise be assessed for their demonstrated effects on combustion and heat removal. Evaluation should record the intervention start relative to venting and cell failure, agent delivery conditions, subsequent cell failures, and temperature and gas-release histories, including the period after agent supply ceases. Extinction of the visible flame is one measured outcome; residual release and possible reignition remain part of the post-extinction assessment.

Table 6. Comparison of representative experiments on early warning and mitigation of lithium-ion battery failure.

Study	Tested Battery System	Initiation and Boundary Conditions	Measurement or Intervention	Reported Result	Implication for Mining Applications
Cui et al. [49]	50 Ah prismatic NMC and LFP cells; 100% SOC	300 W plate heating or chamber heating at 5 °C/min; sealed test tube	Gas release, voltage, temperature and chamber pressure	Reported gas-release-to-TR intervals: 1585 s for NMC and 987 s for LFP; TR defined by a cell temperature-rise rate exceeding 1 °C/s	Demonstrates precursor timing in the reported cell tests; installed-system alarm latency and intervention margins require separate determination
Torres-Castro et al. [50]: diagnostic comparison	11.6 Ah NMC pouch cells; single-cell and parallel/series assemblies; initially 100% SOC	External heating at 5 °C/min or 1C overcharge	Rapid EIS, VOC and other gas sensors	Single-cell warning times: EIS/VOC, 22.5/7.1 min under heating and 7.4/8.5 min under overcharge	Sensor ordering depends on fault mode; warning margins also vary with electrical configuration
Torres-Castro et al. [50]: preventive intervention	Four 11.6 Ah NMC pouch cells in a 1s4p assembly; initially 100% SOC	Overheating or overcharge with controllable abuse inputs	Diagnostic-triggered termination of external heating or charging	No thermal runaway in the reported intervention tests	Demonstrates intervention against removable abuse inputs; does not establish control of self-sustaining internal faults

Ye et al. [106]	3.5 Ah ternary lithium-ion 18650 cells; 50%, 75% and 100% SOC	Filament heating; cell and module immersion tests with different immersion depths	Immersion cooling; temperature and venting observations	Venting-to-TR interval increased from 70 s at 20 mm immersion to 312 s at 70 mm; adjacent cells still vented in propagation tests	Cooling depth affects mitigation; inhibited propagation does not eliminate residual venting hazards
Lee et al. [115]	12–15 LCO 18650 cells; 2.6 Ah per cell; 100% SOC	115 W initiation heater; barrier comparisons under N_2 flow at 186 L/min	5 mm gaps with steel, intumescent or ceramic-fibre barriers	Ceramic-fibre barriers slowed propagation by more than a factor of 30; none completely prevented propagation	Requires validation under combustible atmospheres and representative pack configurations

Diagnostic alarm-to-failure times, gas-release-to-runaway intervals, and venting-to-runaway intervals have different starting points. In Ref. [49], TR is defined by a cell temperature-rise rate exceeding 1 °C/s. The reported precursor intervals do not specify the complete installed-system detection and response delay. Prevention after termination of an abuse input and slowing of propagation also represent different intervention outcomes. Results apply to the reported configurations and should not be used to rank technologies across different abuse protocols. EIS: electrochemical impedance spectroscopy; VOC: volatile organic compounds; TR: thermal runaway.

8.5. Charging and Battery-Swapping Safety with Coordinated Emergency Response

Charging and battery-swapping areas concentrate high-SOC batteries, high-power electrical equipment, and multiple vehicles, making them critical risk locations in an electrified underground mine. Facility siting should compare credible release and fire scenarios at candidate locations, including their effects on occupied areas, shared ventilation paths, and principal escape routes. Separation from combustible storage and hazardous gas areas, where present, should be considered together with firefighting access, equipment spacing, and the handling of disabled vehicles. Guidance from the Global Mining Guidelines Group (GMG) identifies charging layout, environmental conditions, spacing, operation, and local requirements as planning considerations [122]. Simultaneous charging and battery storage should be represented in the site assessment so that the potential for multi-battery exposure and loss of common access or services is evaluated. Battery condition, connectors, and cooling systems should be checked before charging, while vehicles involved in a collision, water ingress, an insulation alarm, or abnormal heating should not proceed directly to fast charging. Battery-swapping systems should retain battery identity, state of health, and fault history. Mechanical interlocks, status verification, and work-zone isolation are also needed to reduce the risks of battery drops, crushing, short circuits, and operating errors [123].

Fixed gas, temperature, smoke, and flame detectors should cover charging areas, battery-storage locations, and zones where vent gases may accumulate. Their positions should reflect the buoyancy and transport characteristics of the target gases rather than using a common installation height for every sensor. Detection data should be linked to vehicle status, personnel location, and ventilation measurements. Early abnormalities may trigger charging interruption or power limitation, whereas confirmed venting, external flames, or continuing propagation require vehicle isolation, personnel evacuation, and assessment of the ventilation response. Xue et al. trained random forest models for fire location and size using MFIRE-generated airflow data from a calibrated ventilation network [124]. With data from five selected airways, the reported fire-location accuracy was 0.920 within the simulated dataset. Prediction was sensitive to fire size and to misleading airflow responses from closely connected airways. These results support scenario-specific model development; performance with field measurements and weakly heating unignited releases requires separate evaluation. Relocation of an abnormal vehicle requires a separate assessment of battery condition, movement-induced loading, the transport route, and

the consequences of a release along that route. The absence of confirmed sustained venting or thermal runaway is not sufficient evidence of safe movability. Continued driving during an escalating incident can aggravate the fault or relocate the source to a position with greater ventilation or evacuation consequences.

Operational reports illustrate how a vehicle fire can restrict access and complicate rescue. During the underground electric boom-truck fire in the Onaping district on 6 July 2020, two contractors initially reported being trapped behind the burning vehicle. Ontario Mine Rescue described dense smoke, extreme heat and communication difficulties during the response. The contractors subsequently passed the vehicle and were provided with breathing apparatus before being transported to the surface [125]. This event highlights the need to account for obstructed routes and loss of communication when planning emergency response.

Battery-related incidents also require identification of the actual failure stage. At Macassa Mine on 14 August 2022, an underground loader repeatedly stalled before smouldering and sparks were observed at its battery. The mine operator attributed the event to a damaged battery connection and explicitly reported that thermal runaway had not occurred [126]. This distinguishes a connection-related incident from confirmed cell thermal runaway. Together, these accounts support attention to connection integrity, route access and communication, while providing no basis for estimating incident frequencies or suppression success rates.

Ventilation response should be evaluated for both smoke-producing fires and unignited battery releases. The absence of a geological flammable-gas hazard in a metal or nonmetal mine does not exclude accumulation of battery-derived fuels. Airflow changes can alter local dilution, cloud movement, heat transfer, and downstream exposure. In gassy coal mines, methane dilution and possible coal-dust entrainment impose additional constraints. The preferred response therefore depends on the source history, fan and regulator states, connected roadways, and personnel distribution.

Candidate ventilation actions should be compared at their expected implementation times, accounting for control and airflow-response delays. Assessment should examine local gas accumulation, heat and contaminant transport, and conditions encountered by personnel at their predicted passage times. Self-rescuer endurance and refuge accessibility should use the time definitions established in Section 7. Rapid explosion-pressure loading requires separate assessment from quasi-steady ventilation adjustment. Monitoring and modelling should be combined to update the scenario and route assessment as conditions change. Table 7 identifies the corresponding protection functions and validation endpoints.

Table 7. Cross-scale protection and validation requirements for battery-electric mining vehicles.

Protection Level	Main Hazard	Core Measures	Control Purpose	Evidence and Application Status	Validation Focus
Cell and monitoring	Latent faults; delayed detection	Cell screening; multi-parameter monitoring; coordinated BMS–BTMS control	Prevent or detect incipient failure; trigger early intervention	Conventional monitoring and protection functions; additional sensing and coordinated intervention require mine-specific validation	Alarm-to-endpoint margin; missed and false alarms; transport and actuation delays; sensor and communication faults
Thermal management	Local hot spots; heat accumulation	Adaptive liquid cooling; immersion cooling; PCM/microcapsule-assisted cooling	Control operating temperature; delay runaway or interrupt propagation where demonstrated	Operating-temperature and selected abuse studies; immersion and encapsulated materials require integrated mining-pack validation	Maximum temperature; temperature difference; heat-removal rate; leakage and cycling stability

Module	Cell-to-cell propagation	Segmentation; barriers; spacing; electrical isolation	Delay or arrest propagation	Configuration-specific propagation tests; effectiveness depends on initiation and discharge paths	Subsequent cell failures; propagation interval; barrier integrity; residual heat and gas discharge
Pack enclosure and structure	Impact; pressure; mass–safety conflict	Lightweight fire-resistant structures; controlled venting; pressure relief; flame arrest	Maintain structural integrity and control release; prevent external ignition where an explosive atmosphere exists	Mining-oriented pressure tests and road-vehicle structural studies; full hybrid-enclosure qualification remains necessary	Mass and mechanical integrity; internal pressure; outlet flow, composition and temperature; blockage; flame passage; post-fire strength
Vehicle	Fire spread; sustained heating; reignition	High-voltage isolation; emergency cooling; fire suppression	Limit vehicle-scale escalation	Established isolation and suppression functions; cooling access and post-extinction stability are pack-dependent	Fire growth; cooling time; reignition; contaminated runoff
Charging and swapping	Multiple high-SOC batteries; handling faults	Separation; interlocks; detection; drainage	Prevent multi-vehicle escalation	Mining guidance and handling studies; installation- and operation-specific assessment	Drop and crush resistance; thermal exposure; smoke removal
Roadway and mine	Unignited gas accumulation; heat and smoke; evacuation failure; methane and dust interaction where present	Smoke and gas monitoring; mine-specific ventilation control; dynamic routing	Limit mine-wide consequences	Experimental and validated transport studies for selected sources; battery-specific and explosion scenarios require separate validation	Local gas accumulation; exposure at passage time; smoke arrival; route viability; applicable evacuation and endurance limits

Figure 9 organises the protective measures around the interfaces between the battery system, vehicle, roadway, and mine response. Escalation across these interfaces is conditional: an unignited battery release can enter a roadway without a sustained vehicle fire, while ignition of secondary vehicle fuels requires sufficient exposure and suitable combustion conditions. Each protection function should therefore be evaluated against the conditions delivered to the next level. A propagation barrier may delay further cell failures while leaving residual gas discharge; pressure relief may reduce enclosure loading while releasing flammable or toxic material; and a ventilation action may improve conditions in one branch while changing exposure elsewhere. Integrated evaluation should retain the event clock and record the resulting heat- and gas-release histories, discharge conditions, ventilation response, and personnel passage times. The framework identifies these assessment relationships; its effectiveness requires evidence that the specified functions and interface conditions are maintained in the representative assembled system and mine scenario.

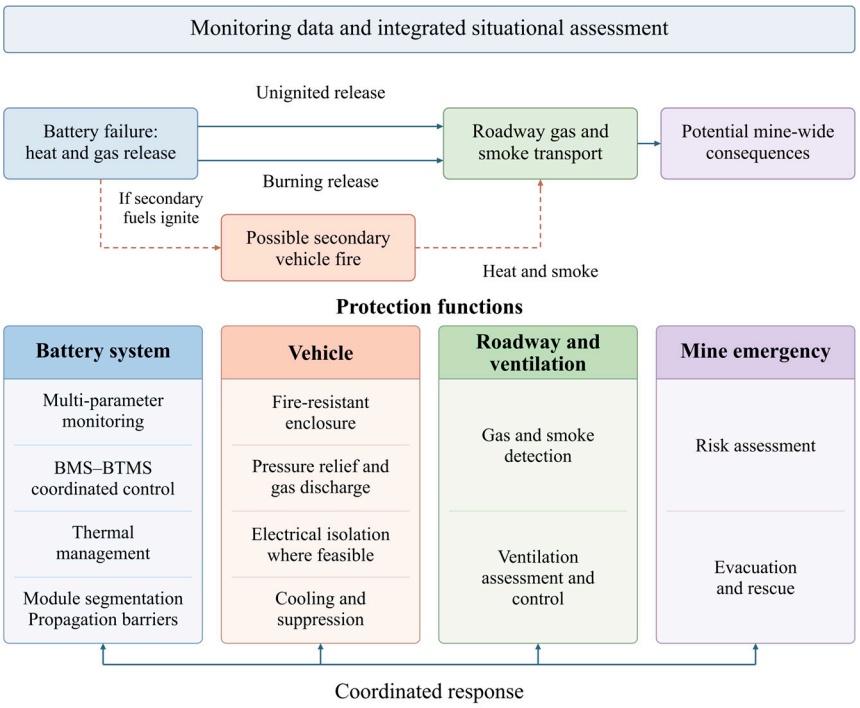


Figure 9. Layered prevention and mitigation framework linking battery monitoring, thermal management, pack-level containment, vehicle control, and mine-wide emergency response.

9. Conclusions and Recommendations

In underground mines, the consequences of battery failure depend on both what the pack releases and where the release travels. Enclosure confinement and venting affect internal pressure and discharge, while mine airflow influences subsequent transport and personnel exposure. Cell and module tests therefore provide a basis for mine-level assessment, but their application requires the release history and the receiving enclosure and roadway conditions to be represented. A measured gas inventory alone cannot determine the pressure history or the exposure encountered during evacuation. Likewise, agreement with contaminant-transport measurements does not by itself establish the ability to predict rapid explosion-pressure loading.

An incident can also escalate without sustained external flames. Heat from failed cells and hot discharge can continue to drive neighbouring-cell failure, while unignited gases may accumulate and create toxic exposure or delayed-ignition hazards. Consequently, the absence or extinction of visible flames is not sufficient evidence that the incident has stabilised. This distinction matters in both coal and metal/non-metal mines. Methane and airborne coal dust can introduce further explosion pathways in gassy coal mines, although their involvement depends on mixing and entrainment conditions. Battery-derived gas hazards remain relevant even where these additional fuels are absent.

The effectiveness of intervention, in turn, depends on the stage of failure. Removing external heating or charging prevented thermal runaway in the reported intervention tests. Once cell reactions become self-sustaining, however, electrical isolation cannot by itself stop heat and gas generation. Cooling and propagation barriers must therefore be considered together with management of the continuing release. Their combined performance depends on which functions remain available after isolation or loss of power and cooling. Thus, the benefit demonstrated by an individual cooling material, barrier, or enclosure design needs to be confirmed within the assembled pack under the relevant incident conditions.

Further work should first establish time-resolved outlet-release histories for mining battery packs and enclosures, with external combustion characterised separately. Measurements of the discharged composition should guide tests of the relevant gas and electrolyte-vapour mixtures, including methane and coal dust where present, to establish their combustion and explosion parameters. Local flow and ventilation-network models then need independent validation against representative transport measurements. The resulting hazard histories should be evaluated at personnel passage times, with alarm delays, usable self-rescuer endurance and refuge accessibility included in route assessment on a common incident clock. By identifying these source inputs and transfer checks, this review connects equipment-level evidence with mine-level safety assessment. Equipment qualification should therefore be combined with site-specific consequence assessment and operational monitoring.

Author Contributions: Conceptualisation, D.W.; methodology, S.L. and Y.S.; investigation, L.Z. and D.W.; visualisation, Y.S.; writing—original draft preparation, S.L.; writing—review and editing, S.L., D.W. and L.Z. All authors have read and agreed to the published version of the manuscript.

Funding: This research was funded by the Special Project for High-Level Talents of China People's Police University (Grant No. BSKYZX202416); the Fundamental Research Funds for the Central Universities (Grant No. 2026JCCXAQ02); the Opening Project of the State Key Laboratory of Explosion Science and Safety Protection, Beijing Institute of Technology (Grant No. KFJJ26-19M); the Hebei Provincial Higher-Education Scientific Research Project (Grant No. ZC2026300); and the Young and Middle-Aged Faculty Scientific Research Innovation Project of China People's Police University (Grant No. ZQN202508).

Institutional Review Board Statement: Not applicable.

Informed Consent Statement: Not applicable.

Data Availability Statement: No new data were created or analysed in this study. Data sharing is not applicable to this article.

Conflicts of Interest: The authors declare no conflicts of interest.

References

1. Kahraman, M.; Düzgün, H.Ş. Safety implications of integrating battery-electric vehicles with ventilation-on-demand in underground mining: A simulation-driven study at Turquoise Ridge Mine. *J. Ind. Saf.* 2026, *in press*. https://doi.org/10.1016/j.jinse.2026.06.001.
2. Meng, L.; Wang, G.; See, K.W.; Wang, Y.; Zhang, Y.; Zang, C.; Zhou, R.; Xie, B. Large-scale Li-ion battery research and application in mining industry. *Energies* **2022**, *15*, 3884. https://doi.org/10.3390/en15113884.
3. Hooli, J.; Halim, A. Battery electric vehicles in underground mines: Insights from industry. *Renew. Sustain. Energy Rev.* **2025**, *208*, 115024. https://doi.org/10.1016/j.rser.2024.115024.
4. Lai, X.; Yao, J.; Jin, C.; Feng, X.; Wang, H.; Xu, C.; Zheng, Y. A review of lithium-ion battery failure hazards: Test standards, accident analysis, and safety suggestions. *Batteries* **2022**, *8*, 248. https://doi.org/10.3390/batteries8110248.
5. Hu, X.; Gao, F.; Xiao, Y.; Wang, D.; Gao, Z.; Huang, Z.; Ren, S.; Jiang, N.; Wu, S. Advancements in the safety of lithium-ion batteries: The trigger, consequence and mitigation method of thermal runaway. *Chem. Eng. J.* **2024**, *481*, 148450. https://doi.org/10.1016/j.cej.2023.148450.
6. Kuslap, E.; Li, J.; Talehatibieke, A.; Hitch, M. Battery electric vehicles in underground mining: Benefits, challenges, and safety considerations. *Energies* **2025**, *18*, 3588. https://doi.org/10.3390/en18143588.
7. Stewart, C.M. Ventilation considerations and modelling of lithium battery fires in underground mining. In *Proceedings of the Australian Mine Ventilation Conference 2022, Gold Coast, QLD, Australia, 10–12 October 2022*; The Australasian Institute of Mining and Metallurgy: Melbourne, VIC, Australia, 2022; pp. 267–276.
8. Li, K.; Wang, Y.; Zhang, Y.; Wang, S.; Zou, X. Multi-risk assessment of mine lithium battery fire based on quantitative factor characterization. *Int. J. Environ. Res. Public Health* **2023**, *20*, 456. https://doi.org/10.3390/ijerph20010456.

9. Department of Mines and Petroleum. *Prevention of Fires in Underground Mines—Guideline*; Resources Safety, Department of Mines and Petroleum: East perth, Australia, 2013; 42pp.
10. Hua, X.; Thomas, A. Effect of dynamic loads and vibrations on lithium-ion batteries. *J. Low Freq. Noise Vib. Act. Control* **2021**, *40*, 1927–1934. https://doi.org/10.1177/14613484211008112.
11. Liu, Y.; Pan, Y.; Wang, H.; Li, H.; Bao, H.; Zhao, Z.; Liu, B. Mechanical issues of lithium-ion batteries in road traffic conditions: A review. *Thin-Walled Struct.* **2024**, *201*, 111985. https://doi.org/10.1016/j.tws.2024.111985.
12. Wang, Z.; Zhao, Q.; Wang, S.; Song, Y.; Shi, B.; He, J. Aging and post-aging thermal safety of lithium-ion batteries under complex operating conditions: A comprehensive review. *J. Power Sources* **2024**, *623*, 235453. https://doi.org/10.1016/j.jpowsour.2024.235453.
13. Said, K.O.; Ray, A.; Kumar, A.R. A perspective on the safety of large-format lithium-ion batteries in underground mining operations: Thermal runaway and its mitigation. *Int. J. Coal Sci. Technol.* **2025**, *12*, 72. https://doi.org/10.1007/s40789-025-00799-w.
14. Zhang, L.; Mu, Z.; Gao, X. Coupling analysis and performance study of commercial 18650 lithium-ion batteries under conditions of temperature and vibration. *Energies* **2018**, *11*, 2856. https://doi.org/10.3390/en11102856.
15. Edge, J.S.; O'kane, S.; Prosser, R.; Kirkaldy, N.D.; Patel, A.N.; Hales, A.; Ghosh, A.; Ai, W.; Chen, J.; Yang, J.; et al. Lithium-ion battery degradation: What you need to know. *Phys. Chem. Chem. Phys.* **2021**, *23*, 8200–8221. https://doi.org/10.1039/D1CP00359C.
16. Spotnitz, R.; Franklin, J. Abuse behavior of high-power lithium-ion cells. *J. Power Sources* **2003**, *113*, 81–100. https://doi.org/10.1016/S0378-7753(02)00488-3.
17. Feng, X.; Ouyang, M.; Liu, X.; Lu, L.; Xia, Y.; He, X. Thermal runaway mechanism of lithium-ion batteries for electric vehicles: A review. *Energy Storage Mater.* **2018**, *10*, 246–267. https://doi.org/10.1016/j.ensm.2017.05.013.
18. Wang, Q.; Mao, B.; Stoliarov, S.I.; Sun, J. A review of lithium-ion battery failure mechanisms and fire prevention strategies. *Prog. Energy Combust. Sci.* **2019**, *73*, 95–131. https://doi.org/10.1016/j.pecs.2019.03.002.
19. Ren, D.; Feng, X.; Liu, L.; Hsu, H.; Lu, L.; Wang, L.; He, X.; Ouyang, M. Investigating the relationship between internal short circuit and thermal runaway of lithium-ion batteries under thermal abuse condition. *Energy Storage Mater.* **2021**, *34*, 563–573. https://doi.org/10.1016/j.ensm.2020.10.020.
20. Finegan, D.P.; Scheel, M.; Robinson, J.B.; Tjaden, B.; Di Michiel, M.; Hinds, G.; Brett, D.J.L.; Shearing, P.R. In-operando high-speed tomography of lithium-ion batteries during thermal runaway. *Nat. Commun.* **2015**, *6*, 6924. https://doi.org/10.1038/ncomms7924.
21. Tschirschwitz, R.; Bernardy, C.; Wagner, P.; Rappsilber, T.; Liebner, C.; Hahn, S.K.; Krause, U. Harmful effects of lithium-ion battery thermal runaway: Scale-up tests from cell to second-life modules. *RSC Adv.* **2023**, *13*, 20761–20779. https://doi.org/10.1039/D3RA02881J.
22. Dubaniewicz, T.H.; Zlochower, I.; Barone, T.L.; Thomas, R.; Yuan, L. Thermal runaway pressures of iron phosphate lithium-ion cells as a function of free space within sealed enclosures. *Min. Metall. Explor.* **2021**, *38*, 539–547. https://doi.org/10.1007/s42461-020-00349-9.
23. Dubaniewicz, T.H.; Barone, T.L.; Brown, C.B.; Thomas, R.A. Comparison of thermal runaway pressures within sealed enclosures for nickel manganese cobalt and iron phosphate cathode lithium-ion cells. *J. Loss Prev. Process Ind.* **2022**, *76*, 104739. https://doi.org/10.1016/j.jlp.2022.104739.
24. Dubaniewicz, T.H. Explosion-proof enclosure failure to contain a lithium-ion battery thermal runaway. *Min. Metall. Explor.* **2025**, *42*, 2499–2506. https://doi.org/10.1007/s42461-025-01288-z.
25. Larsson, F.; Andersson, P.; Blomqvist, P.; Mellander, B.E. Toxic fluoride gas emissions from lithium-ion battery fires. *Sci. Rep.* **2017**, *7*, 10018. https://doi.org/10.1038/s41598-017-09784-z.
26. Baird, A.R.; Archibald, E.J.; Marr, K.C.; Ezekoye, O.A. Explosion hazards from lithium-ion battery vent gas. *J. Power Sources* **2020**, *446*, 227257. https://doi.org/10.1016/j.jpowsour.2019.227257.
27. Qiu, M.; Liu, J.; Cong, B.; Cui, Y. Research progress in thermal runaway vent gas characteristics of Li-ion batteries. *Batteries* **2023**, *9*, 411. https://doi.org/10.3390/batteries9080411.
28. Bugryniec, P.J.; Resendiz, E.G.; Nwophoke, S.M.; Khanna, S.; James, C.; Brown, S.F. Review of gas emissions from lithium-ion battery thermal runaway failure—Considering toxic and flammable compounds. *J. Energy Storage* **2024**, *87*, 111288. https://doi.org/10.1016/j.est.2024.111288.
29. Guo, J.; Guo, Q.; Liu, J.; Wang, H. The polarization and heat generation characteristics of lithium-ion battery with electric–thermal coupled modeling. *Batteries* **2023**, *9*, 529. https://doi.org/10.3390/batteries9110529.
30. Tomaszewska, A.; Chu, Z.; Feng, X.; O'Kane, S.; Liu, X.; Chen, J.; Ji, C.; Endler, E.; Li, R.; Liu, L.; et al. Lithium-ion battery fast charging: A review. *eTransportation* **2019**, *1*, 100011. https://doi.org/10.1016/j.etran.2019.100011.

31. Lin, X.; Khosravinia, K.; Hu, X.; Li, J.; Lu, W. Lithium plating mechanism, detection, and mitigation in lithium-ion batteries. *Prog. Energy Combust. Sci.* **2021**, *87*, 100953. https://doi.org/10.1016/j.pecs.2021.100953.
32. Qu, J.G.; Jiang, Z.Y.; Zhang, J.F. Investigation on lithium-ion battery degradation induced by the combined effect of current rate and operating temperature during fast charging. *J. Energy Storage* **2022**, *52*, 104811. https://doi.org/10.1016/j.est.2022.104811.
33. Xiong, R.; Ma, S.; Li, H.; Sun, F.; Li, J. Toward a safer battery management system: A critical review on diagnosis and prognosis of battery short circuit. *iScience* **2020**, *23*, 101010. https://doi.org/10.1016/j.isci.2020.101010.
34. Ren, D.; Hsu, H.; Li, R.; Feng, X.; Guo, D.; Han, X.; Lu, L.; He, X.; Gao, S.; Hou, J.; et al. A comparative investigation of aging effects on thermal runaway behavior of lithium-ion batteries. *eTransportation* **2019**, *2*, 100034. https://doi.org/10.1016/j.etran.2019.100034.
35. Eroglu, S.E.; Kahraman, M.; Duzgun, H.S. Integrated simulation and network analysis of battery fire risk in underground mining systems. *Reliab. Eng. Syst. Saf.* **2026**, *272*, 112668. https://doi.org/10.1016/j.ress.2026.112668.
36. Wang, Q.; Ping, P.; Zhao, X.; Chu, G.; Sun, J.; Chen, C. Thermal runaway caused fire and explosion of lithium-ion batteries. *J. Power Sources* **2012**, *208*, 210–224. https://doi.org/10.1016/j.jpowsour.2012.02.038.
37. Chen, H.; Buston, J.E.H.; Gill, J.; Howard, D.; Williams, R.C.E.; Rao Vendra, C.M.; Shelke, A.; Wen, J.X.; Wen, X.L. An experimental study on thermal runaway characteristics of lithium-ion batteries with high specific energy and prediction of heat release rate. *J. Power Sources* **2020**, *472*, 228585. https://doi.org/10.1016/j.jpowsour.2020.228585.
38. Ribière, P.; Grugeon, S.; Morcrette, M.; Boyanov, S.; Laruelle, S.; Marlair, G. Investigation on the fire-induced hazards of Li-ion battery cells by fire calorimetry. *Energy Environ. Sci.* **2012**, *5*, 5271–5280. https://doi.org/10.1039/C1EE02218K.
39. Shen, Y.; Zhang, X.; Zou, K.; Wang, C.; Cai, W.; Cao, F.; Liang, L.; Zhang, J.; Liu, D.; Yang, Y.; et al. Multi-parameter thermal runaway and staged gas explosion characteristics of a 228 Ah mining lithium-ion battery. *Appl. Therm. Eng.* **2026**, *302*, 132092. https://doi.org/10.1016/j.applthermaleng.2026.132092.
40. Essl, C.; Golubkov, A.W.; Gasser, E.; Nachtnebel, M.; Zankel, A.; Ewert, E.; Fuchs, A. Comprehensive hazard analysis of failing automotive lithium-ion batteries in overtemperature experiments. *Batteries* **2020**, *6*, 30. https://doi.org/10.3390/batteries6020030.
41. Koch, S.; Fill, A.; Birke, K.P. Comprehensive gas analysis on large-scale automotive lithium-ion cells in thermal runaway. *J. Power Sources* **2018**, *398*, 106–112. https://doi.org/10.1016/j.jpowsour.2018.07.051.
42. Golubkov, A.W.; Fuchs, D.; Wagner, J.; Wiltsche, H.; Stangl, C.; Fauler, G.; Voitic, G.; Thaler, A.; Hacker, V. Thermal-runaway experiments on consumer Li-ion batteries with metal-oxide and olivine-type cathodes. *RSC Adv.* **2014**, *4*, 3633–3642. https://doi.org/10.1039/C3RA45748F.
43. Golubkov, A.W.; Scheikl, S.; Planteu, R.; Voitic, G.; Wiltsche, H.; Stangl, C.; Fauler, G.; Thaler, A.; Hacker, V. Thermal runaway of commercial 18650 Li-ion batteries with LFP and NCA cathodes—Impact of state of charge and overcharge. *RSC Adv.* **2015**, *5*, 57171–57186. https://doi.org/10.1039/C5RA05897J.
44. Yuan, L.; Dubaniewicz, T.; Zlochower, I.; Thomas, R.; Rayyan, N. Experimental study on thermal runaway and vented gases of lithium-ion cells. *Process Saf. Environ. Prot.* **2020**, *144*, 186–192. https://doi.org/10.1016/j.psep.2020.07.028.
45. Amano, K.O.A.; Hahn, S.K.; Butt, N.; Vorwerk, P.; Gimadieva, E.; Tschirschwitz, R.; Rappsilber, T.; Krause, U. Composition and explosibility of gas emissions from lithium-ion batteries undergoing thermal runaway. *Batteries* **2023**, *9*, 300. https://doi.org/10.3390/batteries9060300.
46. Finegan, D.P.; Darcy, E.; Keyser, M.; Tjaden, B.; Heenan, T.M.M.; Jervis, R.; Bailey, J.J.; Malik, R.; Vo, N.T.; Magdysyuk, O.V.; et al. Identifying the cause of rupture of Li-ion batteries during thermal runaway. *Adv. Sci.* **2018**, *5*, 1700369. https://doi.org/10.1002/advs.201700369.
47. Liao, Z.; Zhang, J.; Gan, Z.; Wang, Y.; Zhao, J.; Chen, T.; Zhang, G. Thermal runaway warning of lithium-ion batteries based on photoacoustic spectroscopy gas sensing technology. *Int. J. Energy Res.* **2022**, *46*, 21694–21702. https://doi.org/10.1002/er.8632.
48. Song, Y.; Lyu, N.; Shi, S.; Jiang, X.; Jin, Y. Safety warning for lithium-ion batteries by module-space air-pressure variation under thermal runaway conditions. *J. Energy Storage* **2022**, *56*, 105911. https://doi.org/10.1016/j.est.2022.105911.
49. Cui, Y.; Shi, D.; Wang, Z.; Mou, L.; Ou, M.; Fan, T.; Bi, S.; Zhang, X.; Yu, Z.; Fang, Y. Thermal runaway early warning and risk estimation based on gas production characteristics of different types of lithium-ion batteries. *Batteries* **2023**, *9*, 438. https://doi.org/10.3390/batteries9090438.
50. Torres-Castro, L.; Bates, A.M.; Johnson, N.B.; Quintana, G.; Gray, L. Early detection of Li-ion battery thermal runaway using commercial diagnostic technologies. *J. Electrochem. Soc.* **2024**, *171*, 020520. https://doi.org/10.1149/1945-7111/ad2440.
51. Lamb, J.; Orendorff, C.J.; Steele, L.A.M.; Spangler, S.W. Failure propagation in multi-cell lithium-ion batteries. *J. Power Sources* **2015**, *283*, 517–523. https://doi.org/10.1016/j.jpowsour.2014.10.081.

52. Feng, X.; He, X.; Ouyang, M.; Lu, L.; Wu, P.; Kulp, C.; Prasser, S. Thermal runaway propagation model for designing a safer battery pack with 25 Ah $LiNi_xCo_\gamma Mn_zO_2$ large-format lithium-ion batteries. *Appl. Energy* **2015**, *154*, 74–91. https://doi.org/10.1016/j.apenergy.2015.04.118.
53. Li, H.; Duan, Q.; Zhao, C.; Huang, Z.; Wang, Q. Experimental investigation on thermal runaway and its propagation in a large-format battery module with $Li(Ni_{1/3}Co_{1/3}Mn_{1/3})O_2$ as cathode. *J. Hazard. Mater.* **2019**, *375*, 241–254. https://doi.org/10.1016/j.jhazmat.2019.03.116.
54. Wilke, S.; Schweitzer, B.; Khateeb, S.; Al-Hallaj, S. Preventing thermal runaway propagation in lithium-ion battery packs using a phase-change composite material: An experimental study. *J. Power Sources* **2017**, *340*, 51–59. https://doi.org/10.1016/j.jpowsour.2016.11.018.
55. Huang, Z.; Li, H.; Mei, W.; Zhao, C.; Sun, J.; Wang, Q. Thermal runaway behavior of lithium iron phosphate batteries during penetration. *Fire Technol.* **2020**, *56*, 2405–2426. https://doi.org/10.1007/s10694-020-00967-1.
56. *IEC 60079-1:2026*; Explosive Atmospheres—Part 1: Equipment Protection by Flameproof Enclosures "d". IEC: Geneva, Switzerland, 2026.
57. Wang, H.; Xu, H.; Zhang, Z.; Wang, Q.; Jin, C.; Wu, C.; Xu, C.; Hao, J.; Sun, L.; Du, Z.; et al. Fire and explosion characteristics of vent gas from lithium-ion batteries after thermal runaway: A comparative study. *eTransportation* **2022**, *13*, 100190. https://doi.org/10.1016/j.etran.2022.100190.
58. Wang, Z.; Yu, X.; Ren, F.; Chen, J.; Li, J.; Yin, B.; Shi, B. Characteristics of gas emission and explosion risk for lithium iron phosphate batteries in a proof-confined chamber: Impact of methane concentration and state of charge. *Fuel* **2026**, *408*, 137703. https://doi.org/10.1016/j.fuel.2025.137703.
59. Cashdollar, K.L. Overview of dust explosibility characteristics. *J. Loss Prev. Process Ind.* **2000**, *13*, 183–199. https://doi.org/10.1016/S0950-4230(99)00039-X.
60. Zhou, Y.H.; Bi, M.S.; Qi, F. Experimental research into effects of obstacle on methane–coal dust hybrid explosion. *J. Loss Prev. Process Ind.* **2012**, *25*, 127–130. https://doi.org/10.1016/j.jlp.2011.07.003.
61. Amyotte, P.R.; Mintz, K.J.; Pegg, M.J.; Sun, Y.H. The ignitability of coal dust–air and methane–coal dust–air mixtures. *Fuel* **1993**, *72*, 671–679. https://doi.org/10.1016/0016-2361(93)90580-U.
62. Addai, E.K.; Gabel, D.; Krause, U. Lower explosion limit of hybrid mixtures of burnable gas and dust. *J. Loss Prev. Process Ind.* **2015**, *36*, 497–504. https://doi.org/10.1016/j.jlp.2015.02.014.
63. Addai, E.K.; Gabel, D.; Krause, U. Explosion characteristics of three component hybrid mixtures. *Process Saf. Environ. Prot.* **2015**, *98*, 72–81. https://doi.org/10.1016/j.psep.2015.06.013.
64. Addai, E.K.; Ali, H.; Amyotte, P.; Krause, U. Experimental and theoretical investigation of the lower explosion limit of multiphase hybrid mixtures. *Process Saf. Prog.* **2019**, *38*, e12045. https://doi.org/10.1002/prs.12045.
65. Wu, D.; Zhao, P.; Spitzer, S.H.; Krietsch, A.; Amyotte, P.R.; Krause, U. A review on hybrid mixture explosions: Safety parameters, explosion regimes and criteria, flame characteristics. *J. Loss Prev. Process Ind.* **2023**, *82*, 104969. https://doi.org/10.1016/j.jlp.2022.104969.
66. Cloney, C.T.; Ripley, R.C.; Pegg, M.J.; Amyotte, P.R. Evaluating regime diagrams for closed-volume hybrid explosions. *J. Loss Prev. Process Ind.* **2017**, *49*, 912–918. https://doi.org/10.1016/j.jlp.2017.03.004.
67. Ajrash, M.J.; Zanganeh, J.; Moghtaderi, B. Methane–coal dust hybrid fuel explosion properties in a large-scale cylindrical explosion chamber. *J. Loss Prev. Process Ind.* **2016**, *40*, 317–328. https://doi.org/10.1016/j.jlp.2016.01.009.
68. Wang, Y.; Wang, Z.; Cao, X.; Wei, H. Study on the characteristics and influence factor of methane and coal dust gas/solid two-phase mixture explosions. *Fire* **2023**, *6*, 359. https://doi.org/10.3390/fire6090359.
69. Xu, Y.; Huang, Y.; Ma, G. A review on the effects of different factors on gas explosions in underground structures. *Underground Space* **2020**, *5*, 298–314. https://doi.org/10.1016/j.undsp.2019.05.002.
70. Henriksen, M.; Vågsæther, K.; Lundberg, J.; Forseth, S.; Bjerketvedt, D. Explosion characteristics for Li-ion battery electrolytes at elevated temperatures. *J. Hazard. Mater.* **2019**, *371*, 1–7. https://doi.org/10.1016/j.jhazmat.2019.02.108.
71. Hansen, R. Smoke stratification in a mine drift with a burning mining vehicle. *Min. Technol.* **2022**, *131*, 129–148. https://doi.org/10.1080/25726668.2022.2058816.
72. Nyman, H.; Ingason, H. Temperature stratification in tunnels. *Fire Saf. J.* **2012**, *48*, 30–37. https://doi.org/10.1016/j.firesaf.2011.11.002.
73. Lee, Y.P.; Tsai, K.C. Effect of vehicular blockage on critical ventilation velocity and tunnel fire behavior in longitudinally ventilated tunnels. *Fire Saf. J.* **2012**, *53*, 35–42. https://doi.org/10.1016/j.firesaf.2012.06.013.

74. Xu, Z.; Zhao, J.; Liu, Q.; Chen, H.; Liu, Y.; Geng, Z.; He, L. Experimental investigation on smoke spread characteristics and smoke-layer height in tunnels. *Fire Mater.* **2019**, *43*, 303–309. https://doi.org/10.1002/fam.2701.
75. Yang, D.; Huo, R.; Zhang, X.L.; Zhu, S.; Zhao, X.Y. Comparative study on carbon monoxide stratification and thermal stratification in a horizontal channel fire. *Build. Environ.* **2012**, *49*, 1–8. https://doi.org/10.1016/j.buildenv.2011.09.009.
76. Oka, Y.; Atkinson, G.T. Control of smoke flow in tunnel fires. *Fire Saf. J.* **1995**, *25*, 305–322. https://doi.org/10.1016/0379-7112(96)00007-0.
77. Wu, Y.; Bakar, M.Z.A. Control of smoke flow in tunnel fires using longitudinal ventilation systems—A study of the critical velocity. *Fire Saf. J.* **2000**, *35*, 363–390. https://doi.org/10.1016/S0379-7112(00)00031-X.
78. Hwang, C.C.; Edwards, J.C. The critical ventilation velocity in tunnel fires—A computer simulation. *Fire Saf. J.* **2005**, *40*, 213–244. https://doi.org/10.1016/j.firesaf.2004.11.001.
79. Li, Y.Z.; Lei, B.; Ingason, H. Study of critical velocity and backlayering length in longitudinally ventilated tunnel fires. *Fire Saf. J.* **2010**, *45*, 361–370. https://doi.org/10.1016/j.firesaf.2010.07.003.
80. Wu, Y.; Atkinson, G.T.; Stoddard, J.P.; James, P. Effect of slope on control of smoke flow in tunnel fires. *Fire Saf. Sci.* **1997**, *5*, 1225–1236. https://doi.org/10.3801/IAFSS.FSS.5-1225.
81. Zhou, F.; Wang, D. Backdraft in descensionally ventilated mine fire. *J. Fire Sci.* **2005**, *23*, 261–272. https://doi.org/10.1177/0734904105047915.
82. Hu, D.; Li, Z.; Wang, H.; Xu, H.; Miao, C. Smoke dispersion test and emergency control plan of fire in mine roadway during downward ventilation. *Sci. Rep.* **2023**, *13*, 3683. https://doi.org/10.1038/s41598-023-30779-6.
83. Zhong, W.; Lv, J.; Li, Z.; Liang, T. A study of bifurcation flow of fire smoke in tunnel with longitudinal ventilation. *Int. J. Heat Mass Transf.* **2013**, *67*, 829–835. https://doi.org/10.1016/j.ijheatmasstransfer.2013.08.084.
84. Ding, C.; Chang, D.; Sun, D.; Zou, S. Numerical simulation of the smoke distribution characteristics in a T-shaped roadway. *Fire* **2024**, *7*, 80. https://doi.org/10.3390/fire7030080.
85. Zhu, H.; Qu, B.; Wang, J.; Hu, L.; Yao, Y.; Liao, Q. Numerical study on the smoke movement and control in main roadway for mine fires occurred in branch. *Case Stud. Therm. Eng.* **2023**, *45*, 102938. https://doi.org/10.1016/j.csite.2023.102938.
86. Yuan, L.; Zhou, L.; Smith, A.C. Modeling carbon monoxide spread in underground mine fires. *Appl. Therm. Eng.* **2016**, *100*, 1319–1326. https://doi.org/10.1016/j.applthermaleng.2016.03.007.
87. Zhou, L.; Yuan, L.; Bahrami, D.; Thomas, R.A.; Rowland, J.H. Numerical and experimental investigation of carbon monoxide spread in underground mine fires. *J. Fire Sci.* **2018**, *36*, 406–418. https://doi.org/10.1177/0734904118793891.
88. Said, K.O.; Bhattacharyya, S.; Kumar, A.R. Understanding the evolution of temperature, smoke, and carbon monoxide during thermal runaway of a large-format battery in an underground mine through CFD modeling and deep learning frameworks. *Process Saf. Environ. Prot.* **2026**, *216*, 109228. https://doi.org/10.1016/j.psep.2026.109228.
89. Hong, Y.; Kang, J.; Fu, C. Rapid prediction of mine tunnel fire smoke movement with machine learning and supercomputing techniques. *Fire Saf. J.* **2022**, *127*, 103492. https://doi.org/10.1016/j.firesaf.2021.103492.
90. Purser, D.A.; McAllister, J.L. Assessment of hazards to occupants from smoke, toxic gases, and heat. In *SFPE Handbook of Fire Protection Engineering*, 5th ed.; Hurley, M.J., Ed.; Springer: New York, NY, USA, 2016; pp. 2308–2428.
91. *ISO 13571:2012*; Life-Threatening Components of Fire—Guidelines for the Estimation of Time to Compromised Tenability in Fires. ISO: Geneva, Switzerland, 2012.
92. Chen, P.; Guo, S.; Wang, Y. Human evacuation affected by smoke movement in mine fires. *Int. J. Coal Sci. Technol.* **2016**, *3*, 28–34. https://doi.org/10.1007/s40789-015-0100-3.
93. Fridolf, K.; Nilsson, D.; Frantzich, H. The impact of smoke on walking speed. *Fire Mater.* **2014**, *38*, 744–759. https://doi.org/10.1002/fam.2217.
94. Ronchi, E.; Fridolf, K.; Frantzich, H.; Nilsson, D.; Walter, A.L.; Modig, H. A tunnel evacuation experiment on movement speed and exit choice in smoke. *Fire Saf. J.* **2018**, *97*, 126–136. https://doi.org/10.1016/j.firesaf.2017.06.002.
95. Martell, M.J.; Sammarco, J.J.; Macdonald, B.; Rubinstein, E. Detectability of a self-illuminating lifeline for self-escape in smoke conditions of an underground mine. *Light. Res. Technol.* **2020**, *52*, 64–78. https://doi.org/10.1177/1477153519829187.
96. Lotero, S.; Androulakis, V.; Khaniani, H.; Hassanalian, M.; Shao, S.; Roghanchi, P. Optimizing fire emergency evacuation routes in underground coal mines: A lightweight network flow approach. *Tunn. Undergr. Space Technol.* **2024**, *146*, 105637. https://doi.org/10.1016/j.tust.2024.105637.
97. Bi, L.; Liu, Y.; Zhong, D.; Wen, L. Multi-objective real-time planning of evacuation routes for underground mine fires. *Appl. Sci.* **2024**, *14*, 7521. https://doi.org/10.3390/app14177521.

98. Xiao, M.; Du, C.; Wang, Y.; Wang, J.; Chang, B. Research on smoke diffusion and evacuation routes of mine fires with complex roadway networks. *Case Stud. Therm. Eng.* **2025**, *66*, 105696. https://doi.org/10.1016/j.csite.2024.105696.
99. Kowalski-Trakofler, K.M.; Vaught, C.; Brnich, M.J. Expectations training for miners using self-contained self-rescuers in escapes from underground coal mines. *J. Occup. Environ. Hyg.* **2008**, *5*, 671–677. https://doi.org/10.1080/15459620802333632.
100. Stafford, A.; Brown Requist, K.W.; Lotero Lopez, S.; Gordon, J.; Momayez, M.; Lutz, E. Underground mining self-escape and mine rescue practices: An overview of current and historical trends. *Min. Metall. Explor.* **2023**, *40*, 2243–2253. https://doi.org/10.1007/s42461-023-00863-6.
101. Margolis, K.A.; Kingsley Westerman, C.Y.; Kowalski-Trakofler, K.M. Underground mine refuge chamber expectations training: Program development and evaluation. *Saf. Sci.* **2011**, *49*, 522–530. https://doi.org/10.1016/j.ssci.2010.12.008.
102. Yu, Y.; Vergori, E.; Maddar, F.; Guo, Y.; Greenwood, D.G.; Marco, J. Real-time monitoring of internal structural deformation and thermal events in lithium-ion cell via embedded distributed optical fibre. *J. Power Sources* **2022**, *521*, 230957. https://doi.org/10.1016/j.jpowsour.2021.230957.
103. Sundin, D.W.; Sponholtz, S. Thermal management of Li-ion batteries with single-phase liquid immersion cooling. *IEEE Open J. Veh. Technol.* **2020**, *1*, 82–92. https://doi.org/10.1109/OJVT.2020.2972541.
104. Li, X.; Zhou, Z.; Zhang, M.; Zhang, F.; Zhou, X. A liquid cooling technology based on fluorocarbons for lithium-ion battery thermal safety. *J. Loss Prev. Process Ind.* **2022**, *78*, 104818. https://doi.org/10.1016/j.jlp.2022.104818.
105. Bai, P.; Xu, R.; Liu, M.; Jia, Z.; Sun, Z.; Wang, J.; Zhang, J.; Pei, J.; Zhang, Q.; Wang, J.; et al. Thermal runaway characteristics of LFP batteries by immersion cooling. *ACS Appl. Energy Mater.* **2023**, *6*, 7205–7211. https://doi.org/10.1021/acsaem.3c00904.
106. Ye, Y.; Mao, Y.; Zhao, L.; Chen, Y.; Chen, M. Experimental investigation of thermal runaway behavior and propagation inhibition of lithium-ion battery by immersion cooling. *Appl. Therm. Eng.* **2024**, *256*, 124093. https://doi.org/10.1016/j.applthermaleng.2024.124093.
107. Pakrouh, R.; Hosseini, M.J.; Bahrampoury, R.; Ranjbar, A.A.; Borhani, S.M. Cylindrical battery thermal management based on microencapsulated phase change slurry. *J. Energy Storage* **2021**, *40*, 102602. https://doi.org/10.1016/j.est.2021.102602.
108. Ping, P.; Dai, X.; Kong, D.; Zhang, Y.; Zhao, H.; Gao, X.; Gao, W. Experimental study on nano-encapsulated inorganic phase change material for lithium-ion battery thermal management and thermal runaway suppression. *Chem. Eng. J.* **2023**, *463*, 142401. https://doi.org/10.1016/j.cej.2023.142401.
109. Zhang, W.; Liang, Z.; Yin, X.; Ling, G. Avoiding thermal runaway propagation of lithium-ion battery modules by using hybrid phase change material and liquid cooling. *Appl. Therm. Eng.* **2021**, *184*, 116380. https://doi.org/10.1016/j.applthermaleng.2020.116380.
110. Zhao, Y.; Shi, J.; Wang, K.; Wang, B.; He, C.; Deng, X. Mechanical properties and optimization analysis on battery box with honeycomb sandwich composite structure. *Int. J. Automot. Technol.* **2023**, *24*, 1–14. https://doi.org/10.1007/s12239-023-0001-1.
111. Li, R.; Zhao, Z.; Bao, H.; Pan, Y.; Wang, G.; Liu, B.; Liao, T.; Li, J. Bio-inspired honeycomb structures to improve the crashworthiness of a battery-pack system. *Eng. Fail. Anal.* **2024**, *158*, 108041. https://doi.org/10.1016/j.engfailanal.2024.108041.
112. Zhang, X.; Lin, Q.; Xiao, Y.; Jia, L.; Yang, T.; Wang, L.; Ma, Q.; Wang, B. Top-down design approach of lightweight composite battery pack enclosure for electric vehicles based on numerical modeling and topology optimization. *Polymers* **2025**, *17*, 2897. https://doi.org/10.3390/polym17212897.
113. Sterling, J.; Tattersall, L.; Bamber, N.; De Cola, F.; Murphy, A.; Millen, S.L.J. Composite structure failure analysis post lithium-ion battery fire. *Eng. Fail. Anal.* **2024**, *160*, 108163. https://doi.org/10.1016/j.engfailanal.2024.108163.
114. Höhne, C.-C.; Gettwert, V.; Frank, F.; Kilian, S.; Menrath, A. Bench-scale fuel fire test for materials of rechargeable energy storage system housings. *J. Therm. Anal. Calorim.* **2023**, *148*, 305–313. https://doi.org/10.1007/s10973-022-11725-6.
115. Lee, C.; Said, A.O.; Stoliarov, S.I. Passive mitigation of thermal runaway propagation in dense 18650 lithium ion cell assemblies. *J. Electrochem. Soc.* **2020**, *167*, 090524. https://doi.org/10.1149/1945-7111/ab8978.
116. United Nations Economic Commission for Europe. *UN Regulation No. 100—Uniform Provisions Concerning the Approval of Vehicles with Regard to Specific Requirements for the Electric Power Train, 03 Series of Amendments*; UNECE: Geneva, Switzerland, 2021.
117. *UL 2580*; Standard for Batteries for Use in Electric Vehicles. UL: Northbrook, IL, USA, 2020.
118. *IEC 62619:2022*; Secondary Cells and Batteries Containing Alkaline or Other Non-Acid Electrolytes—Safety Requirements for Secondary Lithium Cells and Batteries for Use in Industrial Applications. IEC: Geneva, Switzerland, 2022.
119. *KA 26-2025*; Safety Specifications for Lithium-Ion Traction Batteries for Underground Mines. National Mine Safety Administration: Beijing, China, 2025. (In Chinese)
120. *GB 48146-2026*; Technical Conditions of Lithium-Ion Traction Battery Applied in Underground Mine. Standards Press of China: Beijing, China, 2026. (In Chinese)

121. Li, L.; Chen, Z.; Lu, Y.; Zang, P.; Wang, Z.; Cheng, Y. Study on the suppression of thermal runaway of lithium-ion battery by water mist with different additives. *Energy Sources Part A* **2023**, *45*, 11349–11362. https://doi.org/10.1080/15567036.2023.2257613.
122. Global Mining Guidelines Group. *Recommended Practices for Battery Electric Vehicles in Underground Mining, Version 3*; Global Mining Guidelines Group: Ottawa, ON, Canada, 2022.
123. Martinetti, A.; Popović, O.; Demichela, M.; Oreste, P.P.; Cvjetić, A.; Milisavljević, V. Safety challenges in battery swapping operations of electric underground mining trucks. *Appl. Sci.* **2025**, *15*, 6763. https://doi.org/10.3390/app15126763.
124. Xue, Y.; Bahrami, D.; Zhou, L. Identifying the location and size of an underground mine fire with simulated ventilation data and random forest model. *Min. Metall. Explor.* **2023**, *40*, 1399–1407. https://doi.org/10.1007/s42461-023-00800-7.
125. Gillett, S. BEV Emergency Response Incident Review and Best Practices. Presentation at the Battery Electric Vehicle Safety in Mines Symposium, Online, 20 January 2021; Ontario Mine Rescue, Workplace Safety North, 2021. Available online: https://www.workplacesafetynorth.ca/sites/default/files/resources/Ontario-Mine-Rescue-BEV-Emergency-Response-Incident-Review-and-Best-Practices.pdf (accessed on 1 Oct 2026).
126. Ladouceur, N. Macassa Mine Battery Fires Summary. Presentation at the Battery Electric Vehicle Safety in Mines Symposium, 15 February 2024; Agnico Eagle Mines, Workplace Safety North, 2024. Available online: https://www.workplacesafetynorth.ca/sites/default/files/2024-02/Agnico-Eagle-BEV-Equipment-Fires-Case-Studies-2024.pdf (accessed on 1 Oct 2026).

Disclaimer/Publisher's Note: The statements, opinions and data contained in all publications are solely those of the individual author(s) and contributor(s) and not of MDPI and/or the editor(s). MDPI and/or the editor(s) disclaim responsibility for any injury to people or property resulting from any ideas, methods, instructions or products referred to in the content.